AlGaN Nanowire Deep-Ultraviolet Light-emitting Diodes with Graphene Electrode

Heemal Parimoo

Department of Electrical and Computer Engineering
McGill University, Montreal, Quebec, Canada

July 2022

A thesis submitted to McGill University in partial fulfillment of the requirement of the degree of **Master of Science**

Abstract

Recent years have shown an increase in the demand for surface-emitting deep-ultraviolet (UV) AlGaN light emitting diodes (LEDs) due to their essential use in water disinfection, and sterilization. Comparing to laterally injected LEDs, vertical injection offers more advantages, however, existing vertical AlGaN UV LEDs are limited to 280 nm. In addition, surface emission is challenging to achieve at very short wavelengths for thin film AlGaN LEDs and switching to a nanowire (NW) format has proven successful in achieving short wavelengths. However, further development of AlGaN NW deep-UV LEDs requires solving the challenge of severe blocking of UV light emission by conventional metal electrodes (e.g., Ti/Au). Graphene is an attractive choice for an electrode due to its high electrical conductivity and high transparency in the entire UV spectrum. Existing studies use graphene as an intermediate layer, which makes it susceptible to degradation during further device structure growth. In this thesis, we demonstrate surface light emission from 240 to 280 nm with AlGaN NW deep-UV LED structures using transferred monolayer graphene as the top electrode. Detailed characterization of graphene electrode, as well as the device performance, including the comparison between devices using graphene and conventional metal electrode, is further investigated. It is found that, despite of improving the device light output power, graphene electrode tends to lead to large contact resistance, due to the nonuniformity of the NW height. This issue could be potentially mitigated by using NWs by selective area epitaxy. This work, therefore, demonstrates a viable path to the fabrication of surface-emitting vertical semiconductor deep-UV LEDs at short wavelengths using graphene on NW technology.

Abrégé

Ces dernières années ont montré une augmentation de la demande de diodes électroluminescentes (LED) AlGaN émettant en surface dans l'ultraviolet profond (UV) en raison de leur utilisation essentielle dans la désinfection et la stérilisation de l'eau. Par rapport aux LED à injection latérale, l'injection verticale offre plus d'avantages, cependant, les LED UV AlGaN verticales existantes sont limitées à 280 nm. De plus, l'émission de surface est difficile à obtenir à des longueurs d'onde très courtes pour les LED AlGaN à couches minces et le passage à un format nanofil (NW) s'est avéré efficace pour obtenir des longueurs d'onde courtes. Cependant, le développement ultérieur des LED UV profondes AlGaN NW nécessite de résoudre le défi du blocage sévère de l'émission de lumière UV par les électrodes métalliques conventionnelles (par exemple, Ti/Au). Le graphène est un choix attrayant pour une électrode en raison de sa conductivité électrique élevée et de sa grande transparence dans tout le spectre UV. Les études existantes utilisent le graphène comme couche intermédiaire, ce qui le rend susceptible de se dégrader lors de la croissance ultérieure de la structure du dispositif. Dans cette thèse, nous démontrons l'émission de lumière de surface de 240 à 280 nm avec des structures LED UV profondes AlGaN NW utilisant du graphène monocouche transféré comme électrode supérieure. La caractérisation détaillée de l'électrode de graphène, ainsi que les performances de l'appareil, y compris la comparaison entre les appareils utilisant du graphène et une électrode métallique conventionnelle, sont étudiées plus en détail. Il a été constaté que, malgré l'amélioration de la puissance de sortie de la lumière du dispositif, l'électrode de graphène a tendance à conduire à une grande résistance de contact, en raison de la non-uniformité de la hauteur NW. Ce problème pourrait être potentiellement atténué en utilisant des NW par épitaxie de zone sélective. Ce travail démontre donc une voie viable vers la

fabrication de LED UV profondes semi-conductrices verticales à émission de surface à courtes longueurs d'onde utilisant le graphène sur la technologie NW.

Preface and author contributions

This thesis evaluates the performance of graphene as the top electrode for surface-emitting vertical AlGaN nanowire (NW) deep-UV LEDs. Apart from the candidate, the work for this thesis has contributions from several other individuals. The candidate and her supervisor, Prof. Songrui Zhao, have worked very closely on the project and experimental setups.

Chapter 1 to Chapter 3 give a brief background and motivation of this thesis, different methods of growing NWs and graphene, including the application of graphene to LEDs, and basic principles of semiconductor LEDs, respectively. The transmittance data for the conventional metal electrodes in Chapter 1 were simulated with Jiaying Lu's assistance. The literature review in Chapter 2 and Chapter 3 were conducted entirely by the candidate. Chapter 4 to Chapter 6 present the fabrication of graphene electrode, results, and discussions on AlGaN NW deep-UV LEDs with graphene top electrode. The growth of the AlGaN NW device structures using molecular beam epitaxy were achieved with the help of Prof. Zhao and Qihua (David) Zhang, and the transfer and patterning of graphene electrodes were performed by the candidate with Prof. Zhao's guidance. The graphene transfer and lithography processes were completed at the McGill Nanotools facility, with training provided by Dr. Zhao Lu and Mr. Jun Li. Chapter 4 presents X-ray photoelectron spectroscopy results, conducted at the McGill Institute for Advanced Materials (MIAM) facility at McGill University, with training provided by Dr. Lihong Shang. Raman spectroscopy measurements from Chapter 4 to Chapter 6 were performed at two facilities, University of Quebec in Montreal (UQAM) with the help of Gwénaël Chamoulaud, and at the Harrington Lab at McGill University with Prof. Matthew J. Harrington and Jenaes Sivasundarampillai's assistance. Scanning electron microscope images and analysis in Chapter 6 were completed under the assistance of Prof. Zhao.

List of publications

1. H. Parimoo, J. Lu, and S. Zhao, “Deep Ultraviolet Light Emission from AlGaN Nanowires with Graphene Electrode,” in *2021 Photonics North (PN)*, May 2021, pp. 1–1.
2. H. Parimoo, Q. Zhang, M. Vafadar, J. Sivasundarampillai, and S. Zhao, “AlGaN nanowire deep ultraviolet light emitting diodes with graphene electrode,” *Appl. Phys. Lett.*, vol. 120, no. 17, p. 171108, Apr. 2022.
3. Q. Zhang, H. Parimoo, E. Martel, and S. Zhao, “Vertical semiconductor deep ultraviolet light emitting diodes on a nanowire-assisted aluminum nitride buffer layer,” *Sci. Rep.*, vol. 12, no. 1, pp. 1–7, 2022.
4. S. Zhao, Q. Zhang, H. Parimoo, and X. Yin, “Recent Progress on Molecular Beam Epitaxy of AlGaN Nanowires for Deep Ultraviolet Light Emitting Devices,” *ECS Trans.*, vol. 108, no. 6, p. 3, 2022.
5. Q. Zhang, H. Parimoo, E. Martel, X. Yin, and S. Zhao, “Vertical AlGaN Deep Ultraviolet Light Emitting Diodes with Polarization Enhanced p-AlGaN Epilayer on Si Substrate,” *ECS J. Solid State Sci. Technol.*, vol. 11, no. 6, p. 066003, 2022.

Acknowledgments

Firstly, I would like to express my utmost gratitude to my supervisor, Professor Songrui Zhao, for giving me the opportunity to work on nanoelectronic devices and materials, a field I was extremely interested in pursuing fresh out of undergrad. Prof. Zhao guided and encouraged me throughout my research and was always there to provide help at any time of the day. I learnt a great deal from him as a graduate student under his wing, and I will carry this knowledge with me throughout my life. Without his support, I could not imagine getting as far in my research as I did, along with the opportunity to present at conferences and publish in a journal.

Secondly, I would like to thank all my peers at Prof. Zhao's lab: Wenqi Liang, David Zhang, Mohammad Vafadar and Xue Yin. They have always been there to help me with every big or small task in the lab. I'm grateful for Xue Yin who helped me get started in the lab, and for David who helped me with my experiments, and for having engaging conversations where I would often lose track of time. I am especially grateful for Wenqi, who was my partner-in-crime for spontaneous coffee-runs, movies and studying long hours in the graduate student office. Additionally, I would like to extend my gratitude to Dr. Zhao Lu, who was extremely patient with me in the cleanroom whenever I needed training, help or life guidance.

Lastly, I would like to acknowledge my friends and family for their continuous support, in-person and remotely. To my closest friends, Olivia, Merry, Alan and Kingsley, thank you for sharing all the fun and stressful times with me, Montreal wouldn't have been the same without you. A special thanks to Merry, who became more like a sister to me. I have laughed the hardest and cried the most with you and made a best friend for life. To all my siblings, I am beyond thankful to all of you for always guiding me when I was lost or wanted a shoulder to cry on. I am eternally grateful to my parents and grandparents, who have been a beacon of light in my life and always encouraged me to follow my dreams.

Table of Contents

Abstract ..... **ii**

Abrégé ..... **iii**

Preface and author contributions ..... **v**

List of publications ..... **vi**

Acknowledgments ..... **vii**

Table of Contents ..... **viii**

List of Figures ..... **x**

List of Tables ..... **xiii**

List of Acronyms ..... **xiv**

Chapter 1: Introduction **1**

1.1 Motivation 1

1.2. Thesis objective 4

1.3. Thesis organization 4

Chapter 2: Literature Review **6**

2.1 AlGaN NW growth mechanisms 6

2.1.1 VLS 7

2.1.2 CVD and MOCVD 7

2.1.3 Plasma-assisted MBE 8

2.2 Graphene growth 10

2.2.1 Graphene growth using CVD 10

2.2.2 Graphene characterization using Raman spectroscopy 11

2.3 Application of graphene to LED devices 13

2.3.1 General transfer process and application of graphene to thin-film LEDs 13

2.3.2 Graphene transfer to the NW top surface post-NW growth 15

2.3.3 Graphene as an intermediate layer for the subsequent NW growth 17

Chapter 3: LED fundamentals **19**

Chapter 4: AlGaN NW deep-UV LEDs with non-patterned graphene electrode **22**

4.1 Growth of AlGaN NW deep-UV LED structures 22

4.2 Graphene transfer 23

4.3 Characterization of transferred graphene 24

4.3.1 XPS 24

4.3.2 Raman spectroscopy 27

4.4 Characterization of AlGaN NW deep-UV LEDs with transferred graphene electrode 28

Chapter 5: AlGaN NW deep-UV LEDs with patterned graphene electrodes **30**

5.1 Graphene electrode patterning 30

5.2 Characterization of AlGaN NW deep-UV LEDs with patterned graphene electrodes 32

5.3. Performance comparison of devices with graphene electrode and metal electrode 33

5.3.1. Light output power and EQE comparison 34

5.3.2. I-V curve comparison 35

Chapter 6: Discussions **37**

6.1. Possible mechanism for large series resistance and limitations of devices with graphene electrode 37

6.2. Graphene degradation analysis using Raman spectroscopy 40

6.3. Graphene transfer challenges: Easy Transfer graphene versus Cu foil graphene 41

Chapter 7: Conclusion and future work **44**

References **46**

List of Figures

Figure 1: (a) Surface-emitting vertical AlGaN NW deep-UV LEDs with conventional metal contacts [22]. (b) Simulated transmission plot for conventional metal electrodes in the deep-UV regime. 3
Figure 2: Different techniques used for growth of III-nitride NWs [40]. 6
Figure 3: CVD chamber with a three-zone setup with Si substrate in the deposition zone where the AlGaN NWs are deposited [43]. 8
Figure 4: (a) Schematic of PA-MBE [53]. (b) Process showing the growth of AlGaN NWs by PA-MBE [54]. 9
Figure 5: (a) Array of nanostructured openings on a Ti mask on GaN template, followed by SAG of GaN NWs. (b) SEM image of SAG GaN NWs [55]. 10
Figure 6: (a) CVD process on Cu foil. (b) Mechanism of graphene formation on Cu foil by CVD [56]. 11
Figure 7: (a) Raman spectra of pristine graphene (top) and defective graphene (bottom) [61]. (b) Dependence of intensity ratio I_{2D}/I_G on number of graphene layers [59]. 12
Figure 8: Schematic of FLG transfer and lithography processes to fabricate GaN-based near-UV LEDs with graphene electrode [29]. 14
Figure 9: SEM image (top) and schematic (bottom) of transferred graphene on top surface of GaN NWs with (a) zero height variation in NWs, (b) 500 nm height variation in NWs [79]. 16
Figure 10: (a) Schematic of GaN-based NW visible-color LEDs with transferred MLG. (b) Top-view SEM of GaN nanorods with MLG [27]. 17
Figure 11: GaN/AlGaN NW LEDs with graphene as intermediate layer emitting at (a) 365 nm with DLG [81] and (b) 350 nm with monolayer graphene [18]. 18
Figure 12: (a) Double heterostructure LED, with a supply of 2.8 V battery. (b) Parabolic electron-hole relations showing spontaneous emission, accompanied by photon emission in the active layer of LEDs [87]. 19
Figure 13: Flowchart depicting the performance parameters used for LED device characterization. 20
Figure 14: I-V characteristics of an ideal and non-ideal LED [86]. 21
Figure 15: (a) Veeco GENxplor system used for the growth of AlGaN NW device structures in this thesis. (b) Schematic of AlGaN NW device structures grown using PA-MBE [91]. 23

Figure 16: Process flow of graphene transfer to AlGaN NW device structures using Easy Transfer graphene from MSE Supplies.....23
Figure 17: Steps for graphene transfer to AlGaN NW device structures using Easy Transfer graphene. (a) Easy Transfer graphene received from MSE Supplies. (b) Release of polymer from the graphene/SL film. (c) Graphene transfer to AlGaN NW device structures. (d) Removal of SL.....24
Figure 18: XPS spectra taken from three regions of the device, as denoted by the legends in the plot. 25
Figure 19: Normalized XPS spectra for C 1s peak for three regions of the sample. 26
Figure 20: Raman spectra of transferred graphene and bare AlGaN NW surface.....27
Figure 21: (a) Probe station setup for electrical and optical measurements. (b) EL spectra of AlGaN NW deep-UV LEDs with the transferred graphene electrode under varying injection currents.....28
Figure 22: (a) EL intensity versus injection current, with inset showing a photo of the light emission from AlGaN NW deep-UV LEDs with the transferred graphene electrode. (b) FWHM and peak wavelength versus injection current. 29
Figure 23: Process flow of graphene transfer to AlGaN NW device structures using graphene on Cu foil [97].....31
Figure 24: Process flow for the fabrication of graphene electrode with different sizes after graphene transfer [97]. 32
Figure 25: EL spectra of AlGaN NW deep-UV LEDs with the transferred graphene electrode under varying injection currents. 32
Figure 26: (a) EL intensity versus injection current with inset showing light emission from AlGaN NW deep-UV LEDs with patterned graphene electrode. (b) FWHM and peak wavelength versus injection current.....33
Figure 27: Comparison of devices with graphene electrode to devices with metal electrode. (a) Light output power versus injection current. (b) EQE versus injection current [97]. 35
Figure 28: I-V characteristics of devices with metal and graphene electrode [97]. 36
Figure 29: SEM of the as-grown NW wafer at a tilting angle of 45° [97]. 37
Figure 30: Statistics for the as-grown NWs showing (a) height distribution and (b) NW top facet diameter distribution [97].....38
Figure 31: SEM images of transferred graphene on AlGaN NWs at (a) small scale, (b) large scale [97]. 39

Figure 32: Raman spectra of devices with graphene electrode and bare AlGaN NW surface showing graphene characteristic peaks, where "#1" and "#2" refer to the spectra measured from two different graphene regions on the same electrode [97]. 40
Figure 33: Raman spectra of devices with graphene electrode, before and after electrical injection.....41
Figure 34: Graphene transfer challenges during delamination from growth substate and re-lamination on desired substrate, accompanied by common issues arising at each step [100]. 42
Figure 35: Graphene transfer to AlGaN NW device structures using (a) Easy Transfer graphene, (b) graphene on Cu foil. 43

List of Tables

Table 1: Work functions of GaN and graphene [26], [78].....15

Table 2: Characteristic peaks obtained using XPS for three regions on the device. 26

List of Acronyms

Al	Aluminum
$AlCl_3$	Aluminum Chloride
AlGaN	Aluminum Gallium Nitride
AlN	Aluminum Nitride
Ar	Argon
Au	Gold
BE	Binding Energy
C-C	Carbon-Carbon bond
CH_4	Methane
CO	Carbon Monoxide
CO_2	Carbon Dioxide
Cu	Copper
CVD	Chemical Vapor Deposition
CW	Continuous Wave
DH	Double Heterostructure
DI	Deionized
DLG	Double-Layer Graphene
EL	Electroluminescence

EQE	External Quantum Efficiency
FLG	Few-Layer Graphene
FWHM	Full Width Half Maximum
Ga	Gallium
$GaCl_3$	Gallium Trichloride
GaN	Gallium Nitride
H_2	Hydrogen gas
HF	Hydrofluoric acid
InGaN	Indium Gallium Nitride
IPA	Iso-Propynyl Alcohol
ITO	Indium Tin Oxide
I-V	Current-Voltage
LED	Light Emitting Diode
MBE	Molecular Beam Epitaxy
MLG	Multi-Layer Graphene
MOCVD	Metal Organic Chemical Vapor Deposition
MQW	Multiple Quantum Well
N_2	Nitrogen gas
NH_3	Ammonia
Ni	Nickel

NW	Nanowire
O_2	Oxygen gas
PA-MBE	Plasma-Assisted Molecular Beam Epitaxy
PMMA	Polymethyl Methacrylate
QCSE	Quantum Confined Stark Effect
RF	Radio Frequency
RIE	Reactive Ion Etching
SAG	Selective Area Growth
SEM	Scanning Electron Microscopy
Si_2N_3	Silicon Nitride
Si	Silicon
SiO_2	Silicon Dioxide
SL	Sacrificial Layer
TE	Transverse Electric
Ti	Titanium
TJ	Tunnel Junction
TM	Transverse Magnetic
UV	Ultraviolet
VLS	Vapor Liquid Solid
XPS	X-ray Photoelectron Spectroscopy

Chapter 1: Introduction

Deep-ultraviolet (UV) light, i.e., emission wavelength ranging from 200 to 300 nm, has important applications in disinfection (air, water and surfaces), sterilization, curing, and gas sensing [1]–[4]. Conventional deep-UV lighting systems make use of mercury lamps. However, mercury waste is hazardous to the environment. The heating issues due to excessive power consumption add to their cost, and at the same time, provide a short lifetime. Light emitting diodes (LEDs) have emerged as an excellent alternative as they are able to overcome the issues faced with conventional UV light sources [5]. Aluminum gallium nitride (AlGaN) has become the material of choice for deep-UV LEDs due to its direct, ultrawide, and tunable bandgap energy between 3.4 and 6.2 eV [5]–[7]. This thesis study is on the development of AlGaN deep-UV LEDs. This chapter will discuss the motivation, objective, and organization of this thesis.

1.1 Motivation

Majority of the surface-emitting UV LEDs to date are grown on substrates like sapphire and aluminum nitride (AlN), which are electrically insulating substrates. This dictates the need for lateral injection in UV LEDs, with the n- and p-contacts on the same side, which leads to current crowding and local heating, among other disadvantages [8], [9]. On the other hand, vertically injected UV LEDs with contacts on top and bottom sides, alleviate these issues by making use of conductive substrates like n-doped silicon carbide and n-GaN [7]. This makes the vertically injected UV LEDs have better current injection, good scalability, simpler fabrication process and effective heat dissipation [10]. On the downside, the mentioned conductive substrates for vertical injection have significant deep-UV light absorption, and GaN also has a large lattice mismatch with high Al content AlGaN alloys, leading to high threading

dislocation densities. For these reasons, substrate removal is necessary. Today, AlN buffer layers are required in the growth of AlGaN deep-UV LED structures, however, there are severe issues and challenges in the laser lift-off removal process of AlN [11], [12]. As a consequence, vertical AlGaN deep-UV LEDs have been limited to 280 nm [11]–[14].

On the other hand, surface emission from AlGaN deep-UV LEDs becomes increasingly difficult as the emission wavelength gets shorter. An increase of the Al composition in AlGaN alloys is required for shorter wavelengths, which leads to the change in the optical polarization from transverse electric (TE) to transverse magnetic (TM). This makes the propagation of emitted light in plane rather than from the top surface, limiting the light extraction efficiency from the top surface, along with the aforementioned lattice mismatch between AlGaN and commonly used substrates [15], [16].

In this context, AlGaN nanowires (NWs) could be a promising platform for short-wavelength surface-emitting vertical semiconductor deep-UV LEDs. In general, NWs have a large surface-to-bulk volume ratio, which makes them better accommodate the lattice strain due to the lattice mismatch with the commonly used substrates. The NW structure helps avoid any dislocations during growth, provided that the NW radius is below a critical value [17]. Any defect generated is directed to the NW sidewalls rather than the vertical growth direction, delivering a near defect-free bulk region [18] [19]. The efficient lattice strain relaxation allows for the use of a wide range of substrates like conductive silicon (Si), or even flexible substrates to fabricate high-quality AlGaN NWs [20]. In addition, NW arrays exhibit a strong scattering effect which leads to an enhanced light extraction of the TM polarized light from the top surface [21].

Using the NW approach, surface-emitting vertically injected AlGaN deep-UV LEDs below 280 nm have been demonstrated in the past [22], [23]. These devices make use of conventional

metal electrodes like nickel/gold (Ni/Au) or titanium/gold (Ti/Au) for the top contact, shown in Figure 1(a), which blocks the light emission from the top surface severely. Figure 1(b) shows the transmission of metal electrodes in the deep-UV regime. For a thin metal layer of 10-20 nm, the light transmission is only 20%-40% [24], [25]. To enhance the light extraction, it is necessary to use a top electrode with higher transparency, compared to conventional metal electrodes.

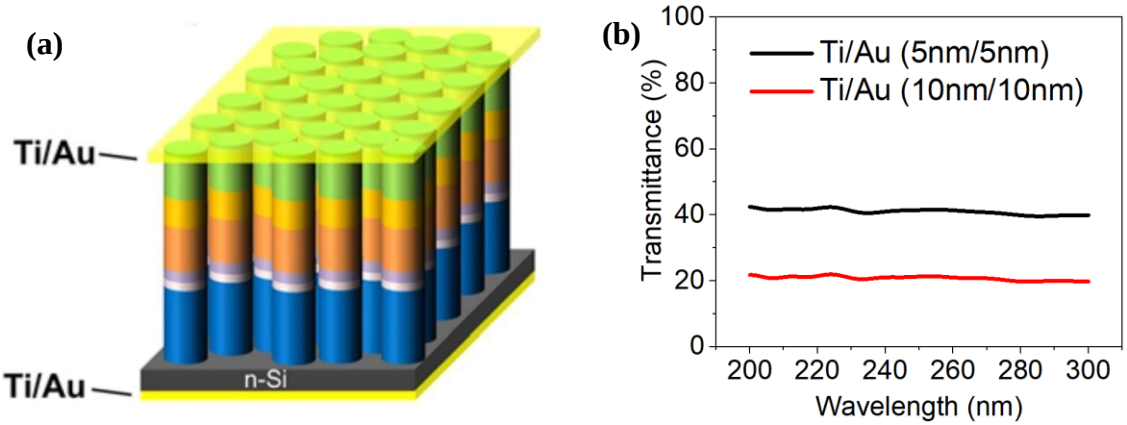

Figure 1: (a) Surface-emitting vertical AlGaN NW deep-UV LEDs with conventional metal contacts [22]. (b) Simulated transmission plot for conventional metal electrodes in the deep-UV regime.

Graphene has emerged as an excellent choice for electrodes [26]–[33]. Graphene is a two-dimensional (2D) allotrope of carbon, arranged in a planar hexagonal geometry of sp^2 carbon [34]. The unique atomic arrangement of the carbon arrays give graphene exceptional properties like near-zero bandgap, high electron mobility of 2×10^5 cm^2/V s at room temperature, low intrinsic resistivity of 30 Ω/sq, and high optical transmittance at all wavelengths [35]–[37]. By being highly conductive and optically transparent, graphene became an enticing material to incorporate in optoelectronic devices as a transparent conductor in photodetectors, solar cells and LEDs [38]. It is worth emphasizing that, compared to conventional metal electrodes,

pristine single-layer graphene (monolayer with thickness of 0.335 nm) only absorbs 2.3% light in the UV region. In other words, pristine graphene has a transmission as high as 97%, which decreases slightly as the number of graphene layer increases (from monolayer to few-layer graphene) [26], [39]. There are, however, no applications of graphene to deep-UV LEDs.

1.2. Thesis objective

This thesis focuses on demonstrating surface light emission in the deep-UV range, between 240 nm and 280 nm, from vertically injected AlGaN NW LEDs, using transferred graphene as the top electrode. This thesis aims to show that graphene electrode is an alternative for the conventional metal electrodes for AlGaN NW UV LEDs in the deep-UV regime.

The objective is achieved by growing AlGaN NW device structures using molecular beam epitaxy (MBE), followed by graphene transfer to the top of the NW surface, and patterning of graphene using standard lithography processes. Structural, electrical, and optical characterizations are performed at each stage of the fabrication, i.e., after the graphene transfer to the AlGaN NW device structures (non-patterned graphene electrode) and after the patterning of the graphene electrode. The characterization techniques include X-ray photoelectron spectroscopy (XPS), Raman spectroscopy, scanning electron microscopy (SEM), current-voltage (I-V) characteristics, electroluminescence studies (EL), and light output power measurements, along with a detailed comparison to devices made with conventional metal electrodes.

1.3. Thesis organization

This section explains the organization of this thesis. Chapter 1 discusses the motivation of this thesis, followed by the objective and organization of this thesis. Chapter 2 first provides a

literature review on different growth techniques of AlGaN NWs and graphene, including characterization techniques of graphene, and then discusses different ways to incorporate graphene to LEDs. Chapter 3 discusses LED fundamentals and their performance parameters. Chapters 1 to 3 prepares the readers with necessary knowledge to understand the research results of this thesis.

Chapters 4 and 5 describe the device structure and performance characteristics, with Chapter 4 focusing on devices with non-patterned graphene electrode, i.e., the graphene electrode is of irregular shape, and Chapter 5 focusing on devices with patterned graphene electrode, i.e., the graphene electrode has a well-defined shape and size. Chapter 5 also includes a comparison of the performance of devices with graphene contacts and metal contacts. Limitation of devices with graphene electrode, as well as a general discussion, regarding to graphene degradation and graphene transfer challenges, is presented in Chapter 6. Chapter 7 summarizes the major conclusions of this thesis, along with possible future developments.

Chapter 2: Literature Review

This chapter provides a literature review on the growth of AlGaN NWs, growth and characterization of graphene using Raman spectroscopy, and application of graphene to LEDs.

2.1 AlGaN NW growth mechanisms

Growth of AlGaN NWs has been studied extensively over the past few years. This section discusses the most popular techniques that have been used in the past, namely, vapor-liquid-solid (VLS), chemical vapor deposition (CVD), metalorganic chemical vapor deposition (MOCVD), and MBE, as shown in Figure 2 [40]. Selective area growth (SAG) using MBE is also discussed.

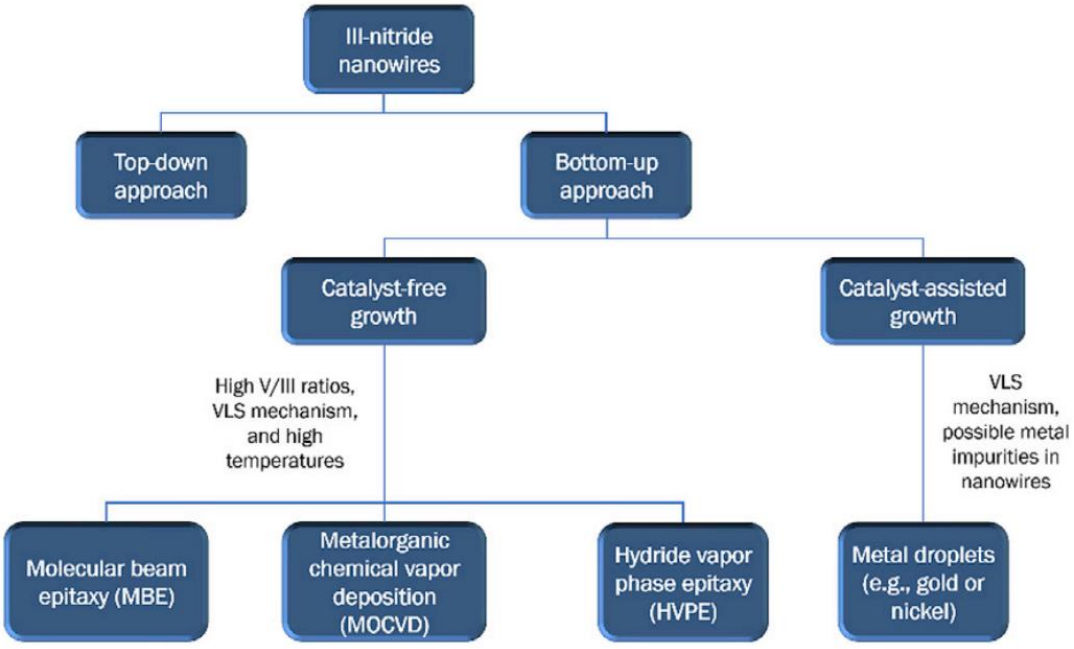

Figure 2: Different techniques used for growth of III-nitride NWs [40].

2.1.1 VLS

NWs can be grown through the VLS technique, with the assistance of a catalyst. In this method, the NWs grow in an anisotropic manner at a liquid-solid interface when the liquid metal catalyst (e.g., Ni or Au for AlGaN NWs) adsorbs a vapor, followed by segregation at the point of supersaturation to form the NWs in the solid phase form [40], [41]. However, VLS growth requires a specific temperature range which depends on the catalyst and the range in which it is most thermodynamically stable [40]. Metal catalysts have also shown to effect the luminescent efficiency due to incorporation of impurities during the NW growth [42]. Thus, the limitations of the VLS growth are primarily due to the involvement of catalysts, and it is evident that a catalyst-free method is required to yield high quality AlGaN NWs.

2.1.2 CVD and MOCVD

CVD follows a VLS mechanism and can be with or without the assistance of a catalyst. Carrier and precursor gases are passed into a chamber with the substrate heated at a high temperature. He et al. synthesized AlGaN NWs on Si substrate by CVD using $GaCl_3$, $AlCl_3$ vapors and ammonia (NH_3) gas at 700 °C, and tuned the Al contents from 0 to 100% [43]. To avoid the problem of phase separation, a three-temperature-zone-tubular furnace was used to separate the partial pressures of $GaCl_3$ and $AlCl_3$, as seen in Figure 3. However, some tapering of the NWs is observed due to the difference in the axial and lateral growth rate [43].

MOCVD is a particular type of CVD technique which makes use of metalorganic, metal hydride and organic compounds [44]. For AlGaN NWs, trimethylgallium, trimethylaluminum, trimethylindium and NH_3 are used as precursors with polycrystalline alumina coated with a thin layer of Ni as the template for growth [45]. MOCVD also enabled growth of multiple quantum well (MQW). Ra et al. synthesized defect-free non-polar core-shell AlGaN NWs with n-Ga core, p-GaN as the shell, cladding layers of AlGaN and MQW in-between [46]. However,

MOCVD requires growth temperatures greater than 1200°C, leading to several issues including the limitation of the substrate choice [47].

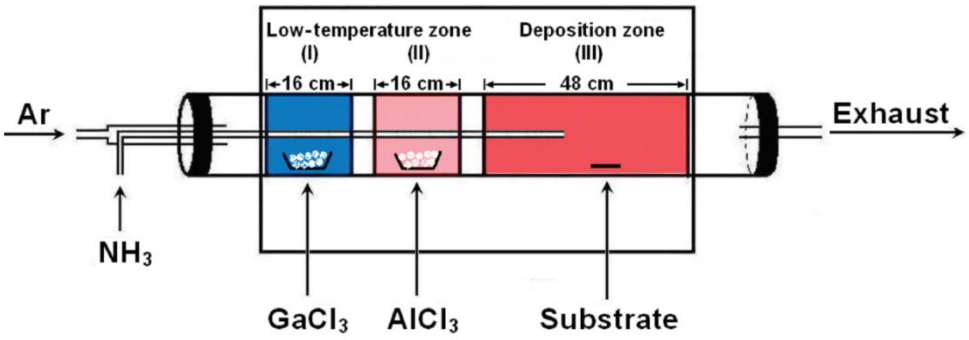

Figure 3: CVD chamber with a three-zone setup with Si substrate in the deposition zone where the AlGaN NWs are deposited [43].

2.1.3 Plasma-assisted MBE

Given the limitations of the aforementioned techniques, plasma-assisted MBE (PA-MBE) has emerged as the most reliable technique for growing AlGaN NWs [22], [23], [48]–[51]. For AlGaN NWs, PA-MBE growth takes place in a vacuum environment with pressures of 10^{-10} mbar (making impurities less susceptible during growth), with a radio frequency (RF) plasma source which supplies active nitrogen species [40], [52]. Unlike the previously mentioned deposition techniques, MBE uses atomic elements as precursors at low fluxes, which are heated in a Knudsen cell, followed by the spraying of the vaporized elements on the substrate, as seen in Figure 4(a) [53]. The growth of the NWs itself is based on a self-organized diffusion process, where the atoms diffuse from the substrate towards the base of the NWs to climb along the lateral sidewalls, as shown in Figure 4(b) [54].

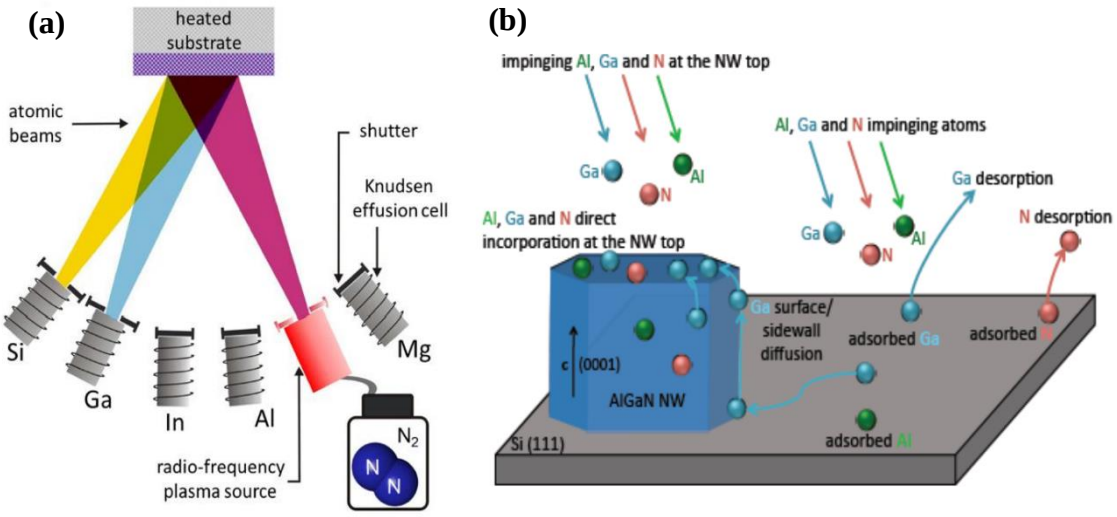

Figure 4: (a) Schematic of PA-MBE [53]. (b) Process showing the growth of AlGaN NWs by PA-MBE [54].

A drawback of the self-organized growth of NWs using PA-MBE is that they grow randomly on substrates, thus, giving a wide distribution of physical properties, such as non-uniform light emission [40]. Due to this reason, SAG has been studied extensively over the past few years. SAG yields NWs with more controlled height, diameter and position, with the help of patterned substrates [40]. Substrates are patterned using e-beam lithography using Si_2N_3, SiO_2 or Ti mask layers, followed by their transfer to the MBE growth chamber for the AlGaN NW growth. Figure 5 shows GaN NWs grown using SAG on a Ti mask with pre-defined geometry, along with the SEM image showing the uniform growth of NWs [55].

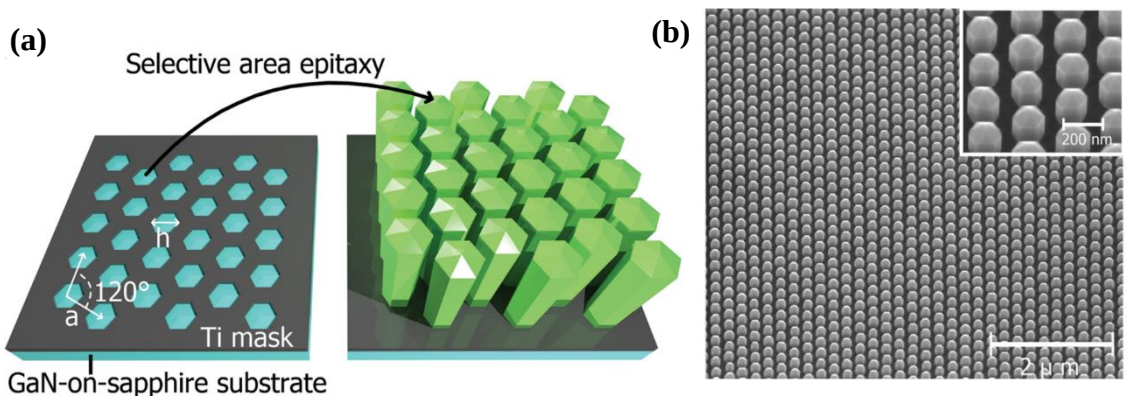

Figure 5: (a) Array of nanostructured openings on a Ti mask on GaN template, followed by SAG of GaN NWs. (b) SEM image of SAG GaN NWs [55].

2.2 Graphene growth

Graphene is synthesized in numerous ways, which can be categorized into top-down and bottom-up approaches. The top-down approach usually refers to methods of exfoliating bulk graphite, using either intercalation, oxidation, or exfoliation methods. On the other hand, the bottom-up approach is an additive process consisting of synthesizing large-area graphene sheets using CVD [56]. This section primarily discusses the bottom-up approach, using CVD. In addition, background on graphene characterization using Raman spectroscopy will also be discussed.

2.2.1 Graphene growth using CVD

Graphene is commonly grown on substrates like copper (Cu) foil, silicon-silicon dioxide (Si/SiO_2) or polymer substrates. Typically, the growth substrate is annealed at 1000 °C in a CVD chamber, followed by introduction of a carbon source, as shown in Figure 6(a) [56]. The combination of high temperature, catalytic properties of the growth substrate and the carbon source, makes the final carbon decompose and dissolve to form graphene on the growth substrate. Different growth substrates have different carbon solubility, i.e., the amount of final carbon product (graphene) that will precipitate will vary, depending on the substrate [38].

The mechanism of growth using CVD differs slightly depending on the substrate used. For example, when using Cu as the growth substrate, the methane gas precursor will catalyze with the Cu, resulting in decomposition of methane and subsequent deposition, nucleation, and polymerization to make graphene, as shown in Figure 6(b). On the other hand, when using Ni as substrate, carbon atoms will dissolve with the Ni at high temperatures, subsequently precipitating out to the surface to make graphene at lower temperatures. The properties of the produced graphene grown on the two mentioned substrates (Cu and Ni) will also differ slightly, as the synthesized graphene quality and performance depends on the precursors used, growth time, and substrate type [56].

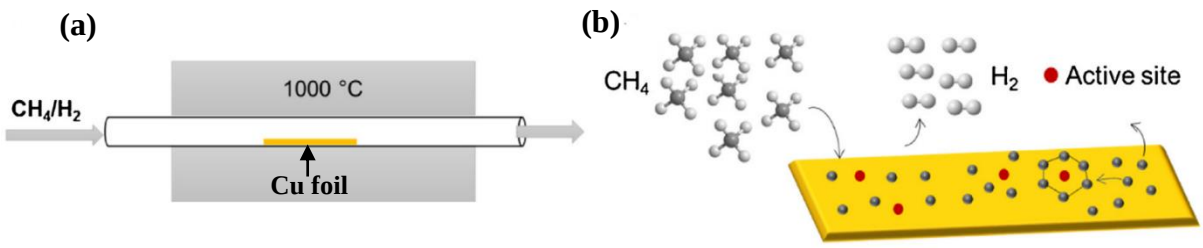

Figure 6: (a) CVD process on Cu foil. (b) Mechanism of graphene formation on Cu foil by CVD [56].

2.2.2 Graphene characterization using Raman spectroscopy

A plethora of techniques, such as Raman spectroscopy, SEM, XPS, optical microscope, have been used in the past to characterize graphene (e.g., thickness, number of layers, quality of deposition) [27], [57]–[60]. However, Raman spectroscopy has emerged as the most common technique for graphene analysis as it is able to detect any small changes in electronic properties due to defects and doping [61]. Figure 7(a) shows all the possible peaks that can be observed in graphene.

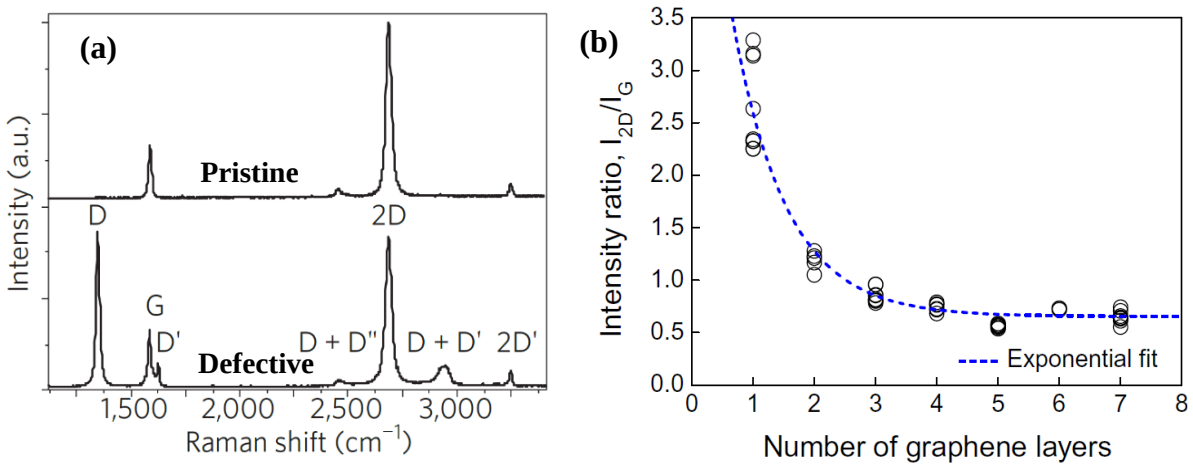

Figure 7: (a) Raman spectra of pristine graphene (top) and defective graphene (bottom) [61]. (b) Dependence of intensity ratio I_{2D}/I_G on number of graphene layers [59].

The D-peak and D'-peak are defect related peaks and indicate impurities or disorders in graphene. Literature shows that the type of defects (vacancy-like defects, boundary-like defects, and etc.) can further be identified using the intensity ratio $I_D/I_{D'}$ [62], [63]. Thus, depending on the quality of the graphene, these peaks might not always be present in the Raman spectrum. However, the G- and 2D- peak will always be present in any graphene and are sensitive to the number of graphene layers. The G-peak is due to the in-plane bond vibration of the sp^2 C-C bond (first-order Raman scattering process), whereas the 2D-peak is generated due to a 2-phonon, second-order Raman scattering process [64]. The D+D"-peak (occasionally referred as the G*-peak) and 2D'-peak are similar to the 2D-peak, in the sense that they are double resonance peaks as well [61], [64]–[66]. Lastly, the D+D'-peak is also a defect-related peak, only seen in defective graphene, and it is assisted by a 2-phonon scattering process [61].

Figure 7(b) plots the dependence of the thickness of graphene layers on the intensity ratio of the 2D- and G-peaks (I_{2D}/I_G) [59]. It is observed that the ratio decreases with the increase in the number of graphene layers, and the largest ratio recorded in Figure 7(b) is 3.5 for monolayer

graphene. However, I_{2D}/I_G ratios greater than 4 have also been observed for monolayer graphene in literature [67]–[69].

2.3 Application of graphene to LED devices

In this section, we describe the application of graphene to LED devices. In Section 2.3.1, general graphene transfer process, together with the existing studies on the application of graphene to thin-film LEDs, is discussed. In Sections 2.3.2 and 2.3.3, the application of graphene to NW LEDs is discussed, with Section 2.3.2 focusing on transferred graphene and Section 2.3.3 focusing on using graphene as an intermediate layer for the subsequent NW device structure growth.

2.3.1 General transfer process and application of graphene to thin-film LEDs

The integration of graphene to LED devices is commonly accomplished using a graphene transfer process. Graphene transfer refers to the transfer of graphene from a growth substrate to the desired substrate. There are three basic steps involved in a graphene transfer. The first step consists of growth of graphene using CVD on a given substrate. The second step involves delamination of the graphene from the growth substrate. This step can be either dry or wet. The dry approach generally uses thermal release tape to delaminate graphene from the growth substrate, and has been used to transfer graphene to substrates like SiO_2/Si, polymer substrates, and Al_2O_3 and GaN [70], [71]. On the other hand, the wet approach makes use of solvents like etchants or water to strip away the growth substrate and facilitate transfer. The wet approach is the primary approach used for graphene transfer to LED device structures. The final step is the lamination of graphene on the target substrate.

In the past, numerous studies have been carried out using transferred graphene as the top electrode for GaN-based thin film devices [26], [28]–[31], [72]–[75]. These devices emit light

in the near-UV or visible region. For example, Kim et al. demonstrated transferred few-layer graphene (FLG) as an electrode for GaN-based thin film near-UV LEDs. The transfer process is shown in Figure 8, where the FLG was grown using CVD on a Cu foil. After etching the Cu foil, the FLG film was transferred to the p-GaN top surface of the LED device structure, followed by etching to deposit contact pads [29].

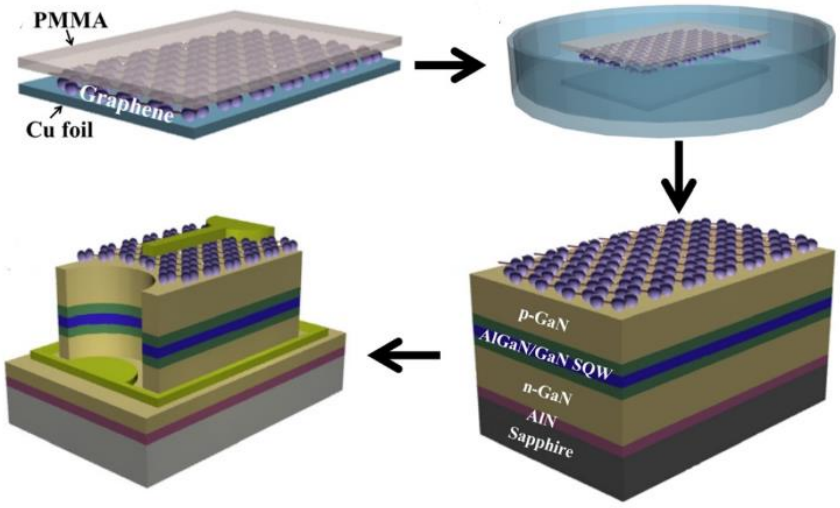

Figure 8: Schematic of FLG transfer and lithography processes to fabricate GaN-based near-UV LEDs with graphene electrode [29].

Even though graphene has prevailed as an appealing candidate to replace metal electrodes for GaN-based LED devices, wet transfer of graphene to LEDs typically does not yield ideal results. Graphene films have many sources of scattering originating from defects, wrinkles and from domain boundaries, arising from the transfer techniques. These defects increase the sheet resistance of monolayer graphene from 30 Ω/sq to 75-1000 Ω/sq [38], [76]. Furthermore, there is a large work function difference between graphene and p-GaN – the most commonly used contact layer in GaN-based LEDs, as seen from Table 1. This mismatch in work function creates an interface contact barrier which further hinders the transport of electrons and holes, increasing contact resistance and operating voltage in LED devices [26], [76]–[78].

Table 1: Work functions of GaN and graphene [26], [78].

Material	**n-GaN**	**p-GaN**	**Pristine graphene**
Work function	~ 4.0 eV	~7.5 eV	~ 4.47 eV

2.3.2 Graphene transfer to the NW top surface post-NW growth

Limited studies report successful transfer of graphene to NW top surface [27], [32], [79], [80]. First, NWs are grown on a substrate using one of the techniques described in Section 2.1, followed by an optional oxygen plasma cleaning and wet etching step, to remove any residues and surface oxides, respectively. Next, graphene transfer to the top surface of the NWs is carried out immediately, using the wet transfer process described earlier. However, this process faces certain challenges. Apart from the challenges arising from the graphene transfer process, the transfer of graphene to NW top surfaces can be uneven due to non-uniform NW height.

For example, Babichev et al. described various defects like blisters and ripples on FLG transferred to a GaN NW UV photodetector [32]. Tearing of the four-layer graphene was reported by NWs which exceeded the average NW length by 100 nm [32]. Similarly, Kierdaszuk et al. presented detailed studies of graphene transferred to GaN NWs where the NWs exhibited variations in height [79]. Figure 9 shows the comparison of NWs with a height variation of 0 (N0) and 500 nm (N500). It is observed that the graphene on NWs with equal NW height in Figure 9(a) show a smooth graphene transfer, with no obvious cracks and wrinkles. However, Figure 9(b) shows visible wrinkles and bends in the graphene film when transferred to NWs with a 500 nm height variation [79]. They have further reported that defects on graphene due to differences in NW morphology (difference in height and density of NWs) can cause strain on the transferred graphene layer, which influences device performance like change in carrier concentration [79]. In addition, the presence of defects on graphene can also

cause an increase in its sheet resistance due to an increase in carrier scattering [18], [38], [81], [82].

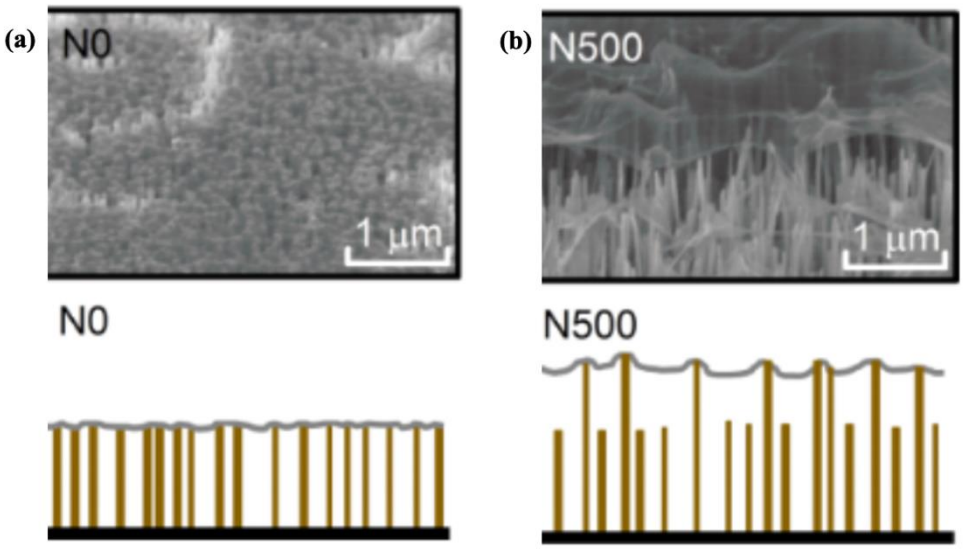

Figure 9: SEM image (top) and schematic (bottom) of transferred graphene on top surface of GaN NWs with (a) zero height variation in NWs, (b) 500 nm height variation in NWs [79].

Using transferred graphene as a conductive electrode, Li et al. demonstrated NW LEDs emitting at 456 nm [27]. In this study, MOCVD was used to grow the device structure, followed by wet transfer of multi-layer graphene (MLG) to the GaN nanorods (Figure 10). To date, however, there are no experimental demonstrations of NW UV LEDs using transferred graphene as the top electrode.

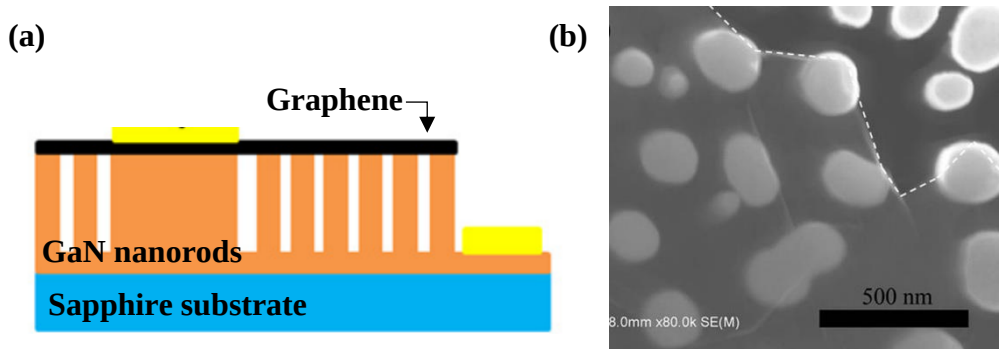

Figure 10: (a) Schematic of GaN-based NW visible-color LEDs with transferred MLG. (b) Top-view SEM of GaN nanorods with MLG [27].

2.3.3 Graphene as an intermediate layer for the subsequent NW growth

Graphene has also been used as an intermediate layer in NW LED devices, i.e., growing the NW LED structures on graphene [18], [81], [83]–[85]. In this case, most of the devices are in "flip-chip" configuration, i.e., light emission occurs from the graphene side rather than the top contact. For example, Hoiaas et al. demonstrated the growth of GaN/AlGaN NWs on a double-layer graphene film (DLG) on silica glass, and further showed UV LEDs at 365 nm, as illustrated in Figure 11(a) [81]. Mulyo et al. demonstrated growth of GaN/AlGaN NWs on monolayer graphene and devices emitting at 350 nm, as shown in Figure 11(b) [18]. However, the graphene film encountered severe damage during the growth of NW device structures, due to the use of nitrogen plasma during the growth. To mitigate this issue, AlN protection layer has been used [83], [84]. Although success was achieved in protecting the graphene layer from impinging nitrogen species using AlN, issues like lattice mismatch (between AlN and graphene) and alteration in the electrical properties of graphene arose.

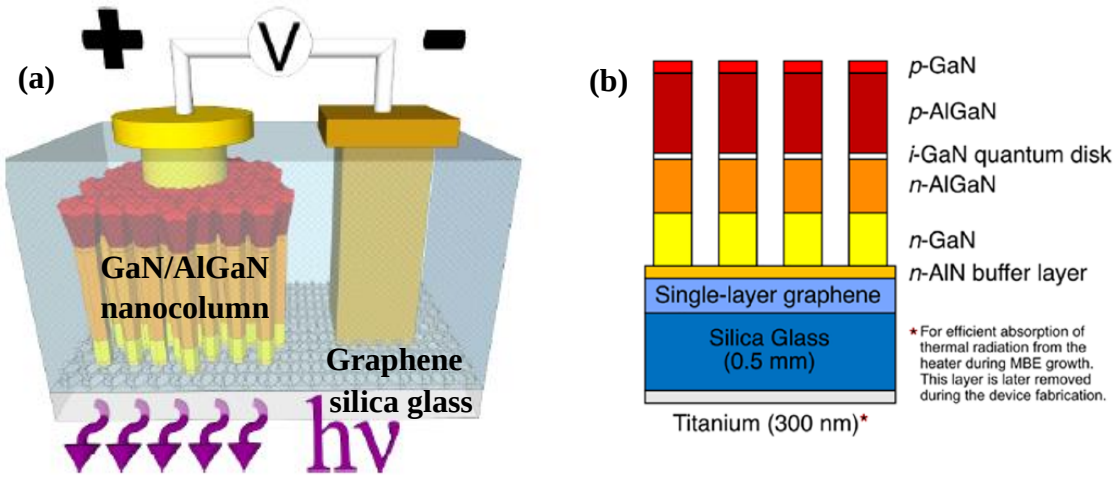

Figure 11: GaN/AlGaN NW LEDs with graphene as intermediate layer emitting at (a) 365 nm with DLG [81] and (b) 350 nm with monolayer graphene [18].

Chapter 3: LED fundamentals

Light emission from LEDs is due to spontaneous recombination of electron-hole (e-h) pairs [86]. Figure 12(a) illustrates a double heterojunction (DH) LED. Figure 12(b) depicts the recombination process of the e-h pair in the active region of a DH structure, wherein the bandgap of the active layer is smaller than that of the n- and p-type layers [87]. The light emission is from the active layer, and the emitted photon energy is approximately the band gap energy, due to the energy conservation. For a semiconductor alloy like $Al_xGa_{1-x}N$, the bandgap can be varied from 3.4 eV (x_{Al} = 0) to 6.2 eV (x_{Al} =1) [6]. Thus, AlGaN can achieve a wide emission spectrum in the UV regime, approximately from 200 nm to 365 nm.

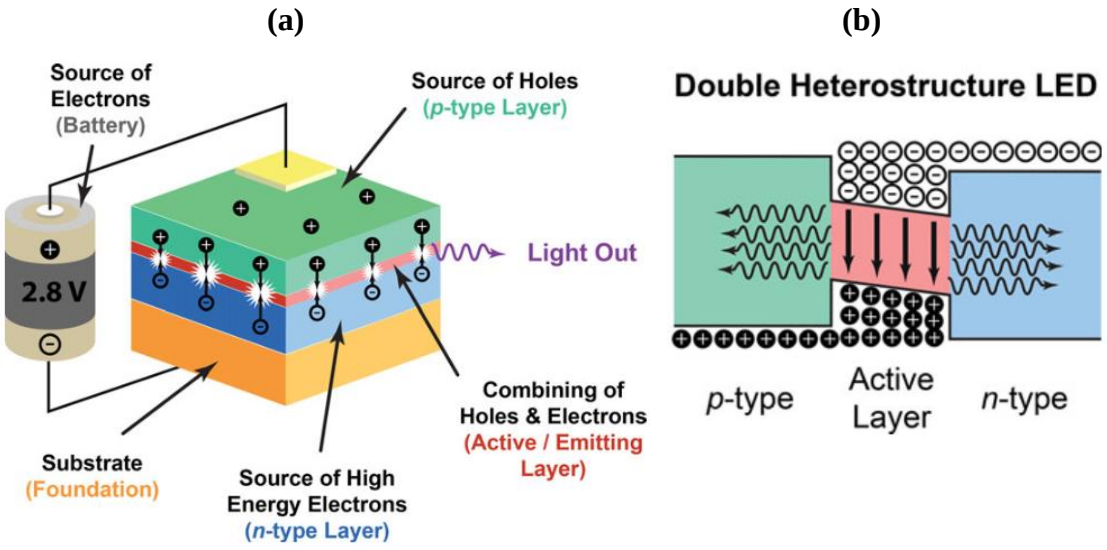

Figure 12: (a) Double heterostructure LED, with a supply of 2.8 V battery. (b) Parabolic electron-hole relations showing spontaneous emission, accompanied by photon emission in the active layer of LEDs [87].

In general, for LED device characterization, various performance parameters can be measured, which can be divided into electrical and optical measurements, illustrated in Figure 13.

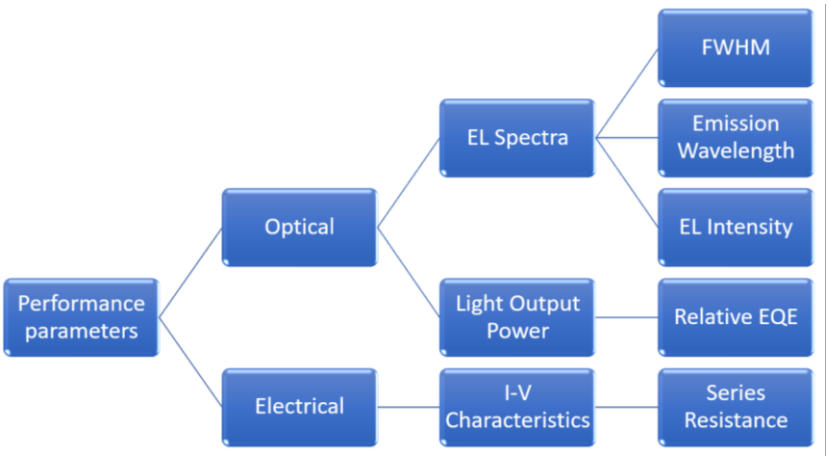

Figure 13: Flowchart depicting the performance parameters used for LED device characterization.

The most common electrical measurement for LEDs is measuring the I-V characteristics. Figure 14 shows the difference between an ideal and non-ideal I-V curve, where the non-ideal I-V curve is due to parasitic resistances [86]. Parasitic resistances refer to the effects of series and parallel resistance on a diode. Series resistance is caused by excessive contact resistance whereas parallel resistance is due to the unwanted electrical conduction channels that are parallel to the p-n junctions, such as surface channel. In this work, series resistance is studied on the AlGaN NW deep-UV LEDs. The series resistance is approximately estimated by taking the tangent (slope) to the I-V curve at large forward bias [86].

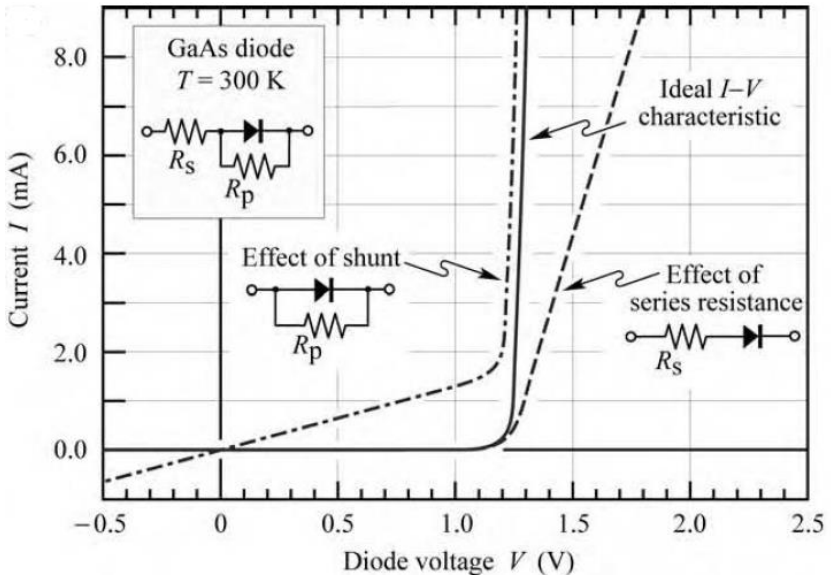

Figure 14: I-V characteristics of an ideal and non-ideal LED [86].

Optical measurements for LEDs include EL and light output power measurements. EL is generated by photons from the excess e-h pair recombination under a forward bias of the p-n junction [4]. EL spectrum allows one to determine the characteristic wavelength of an LED device, and other parameters such as full-width-half-maximum (FWHM) [5]. Light output power measurements allow one to estimate the external quantum efficiency (EQE) of an LED device, which is an important parameter to evaluate the efficiency of an LED device and typically estimated by taking the ratio of the number of photons emitted from the LED device in free space to the number of electrons injected into the device [90].

Chapter 4: AlGaN NW deep-UV LEDs with non-patterned graphene electrode

In this chapter, AlGaN NW deep-UV LEDs with non-patterned graphene electrode are described, i.e., the transfer yields graphene with irregular shape on the top surface of the NW [91]. This is to examine whether the transferred graphene can serve as the top electrode for NW deep-UV LEDs, an essential step toward fabricating patterned graphene electrodes.

4.1 Growth of AlGaN NW deep-UV LED structures

The AlGaN NW device structures in this thesis were grown using a Veeco Genxplor PA-MBE system on highly conductive n-Si substrates. Figure 15(a) shows a photo of the MBE system. Figure 15(b) shows the schematic of the device structure [91]. From the bottom to the top, the NW structure consists of the n-GaN template, tunnel junction (TJ) made of n^+-GaN and p^+-AlGaN, AlGaN DHs which consist of p-AlGaN, n-AlGaN, and undoped AlGaN, and a thin n-GaN top contact layer. Prior to the MBE growth, the Si wafers were cleaned with isopropyl alcohol (IPA), followed by the removal of surface oxides using hydrofluoric acid (HF) and thermal outgassing *in situ* in the MBE chamber. The AlGaN segments were grown at 850-890 °C. Al and Ga fluxes were around 1-2 × 10^{-8} Torr and 0.8-1.5 × 10^{-8} Torr, respectively. The nitrogen flow rate was 0.6 sccm. The TJ growth used a lower substrate temperature of 630 °C.

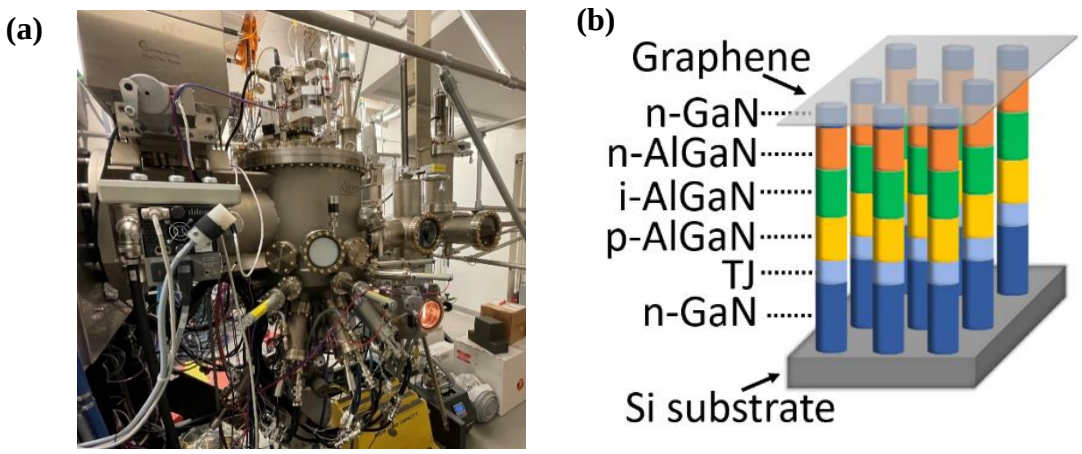

Figure 15: (a) Veeco GENxplor system used for the growth of AlGaN NW device structures in this thesis. (b) Schematic of AlGaN NW device structures grown using PA-MBE [91].

4.2 Graphene transfer

Easy Transfer graphene from MSE supplies was used. The monolayer graphene is sandwiched between a 100 µm porous polymeric material and a 100 nm acrylate-based sacrificial layer (SL). Figure 16 illustrates a schematic of the graphene transfer protocol provided by MSE Supplies.

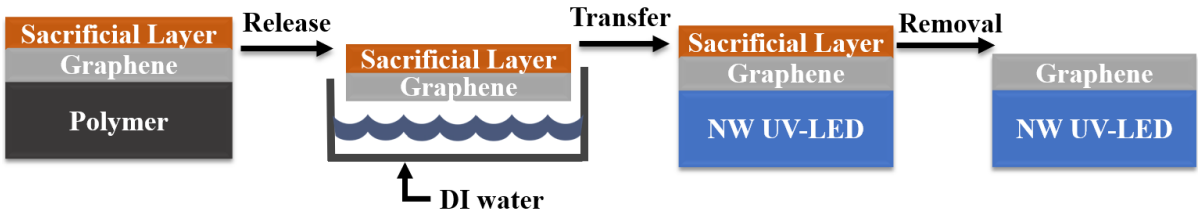

Figure 16: Process flow of graphene transfer to AlGaN NW device structures using Easy Transfer graphene from MSE Supplies.

The first step was submerging the polymer/graphene/SL stack in deionized (DI) water, which led to the release of the graphene/SL film from the polymer film. This led to the graphene/SL film floating in the DI water, ready for transfer to the desired substrate. The

AlGaN NW device structure was introduced into the DI water at a tilted angle of 45°, and the graphene/SL was scooped from the DI water. After the transfer step, the NW UV LED/graphene/SL device was air-dried for 30 minutes, followed by annealing at 95 °C for 1 hour. In the end, the SL was removed by dipping the NW UV LED/graphene/SL device in acetone overnight, followed by washing with IPA and DI water, and dried by N_2 gas. Figure 17 illustrates the graphene transfer that was carried out. It can be seen that the transferred graphene in Figure 17(d) has an irregular shape, with visible cracks.

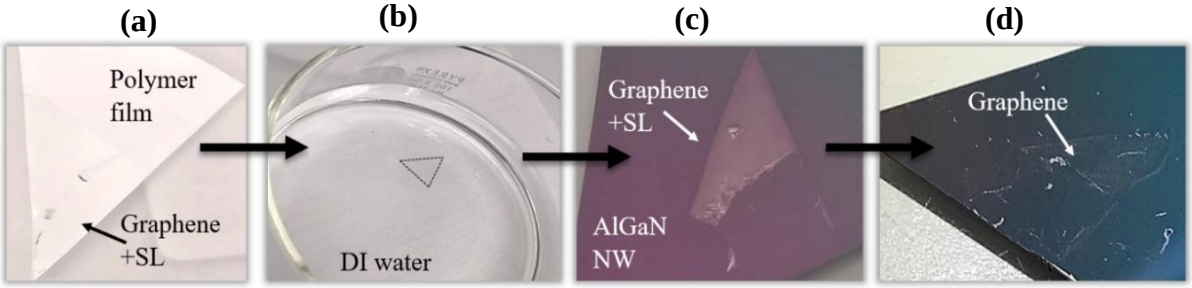

Figure 17: Steps for graphene transfer to AlGaN NW device structures using Easy Transfer graphene. (a) Easy Transfer graphene received from MSE Supplies. (b) Release of polymer from the graphene/SL film. (c) Graphene transfer to AlGaN NW device structures. (d) Removal of SL.

4.3 Characterization of transferred graphene

After graphene transfer, XPS and Raman spectroscopy were performed to inspect if the graphene transfer was successful. Characterization results are described in this section.

4.3.1 XPS

XPS was performed using the Thermo Scientific K-Alpha XPS instrument, with a monochromatic Al α source (hv = 1486.7 eV). The binding energy was calibrated based on the peak of the adventitious carbon, i.e., the C 1s peak at 284.8 eV. Figure 18 shows the survey

spectra scan of binding energy (BE) obtained for three regions on the device, at a pass energy of 200 eV. All regions of the device show the expected characteristic peaks of Ga 3d, Al 2p, N 1s, O 1s and C 1s [58], [92], [93].

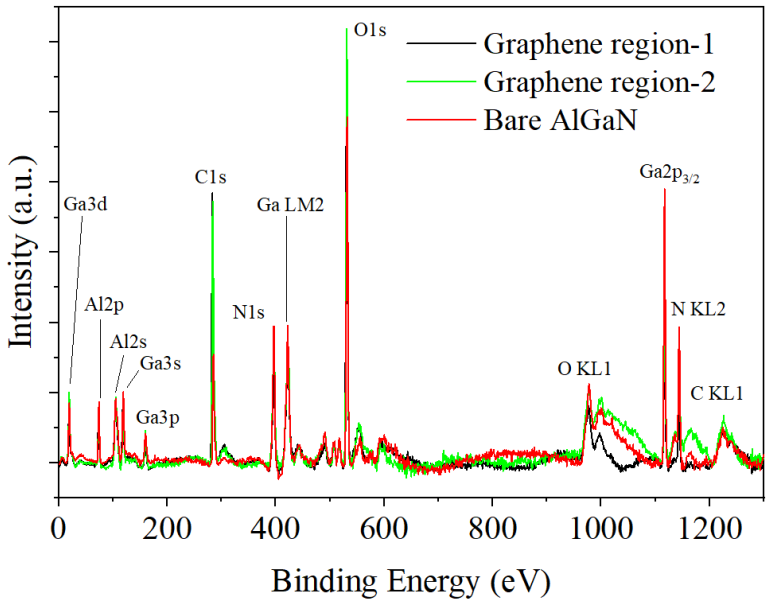

Figure 18: XPS spectra taken from three regions of the device, as denoted by the legends in the plot.

An additional peak at 310 eV was found for all three regions on the device, as seen in Figure 19, with the intensity of the peak being marginally higher for the graphene regions, when compared to the bare AlGaN NW surface. This peak is termed as the "shake-up satellite peak" in literature. It usually corresponds to the π-π^* transition occurring in a sp^2-carbon six-membered ring [58].

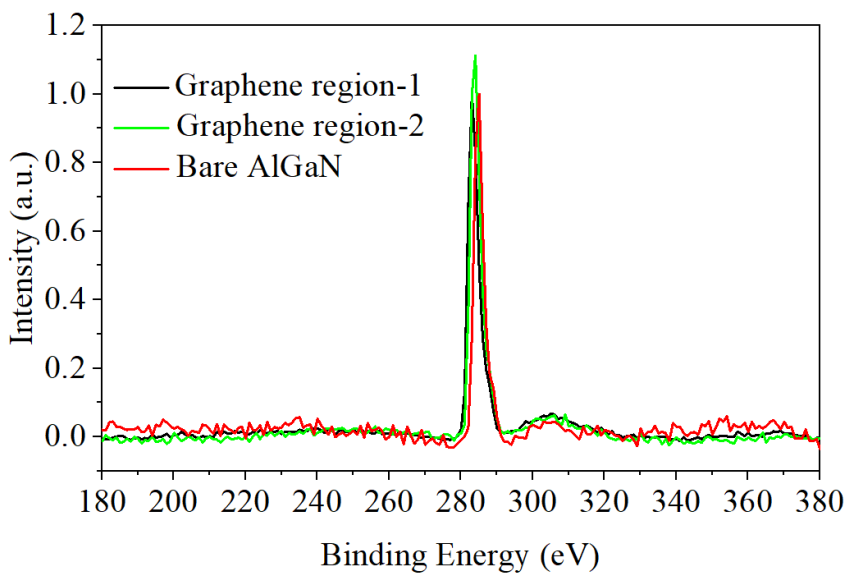

Figure 19: Normalized XPS spectra for C 1s peak for three regions of the sample.

Table 2 summarizes the BE of the peaks observed (after carbon correction) and the corresponding BE reported in literature. The BE of the graphene regions are slightly shifted to higher energy, when compared with the BE of the bare AlGaN NW surface. This indicates that the surface is not bare AlGaN and has been altered due to deposition or transfer of an external material.

Table 2: Characteristic peaks obtained using XPS for three regions on the device.

Element	Graphene region-1 (eV)	Graphene region-2 (eV)	Bare AlGaN NW surface (eV)	Literature (eV)
C 1s		284.8		
Ga 3d	20.34	20.01	19.05	19.00
N 1s	397.61	397.31	396.49	398.00
O 1s	532.38	532.03	531.75	531.00
Al 2p	74.66	74.65	73.76	73.00

4.3.2 Raman spectroscopy

Further characterization of the transferred graphene was performed by Raman spectroscopy (Renishaw Raman instrument). A 532 nm green laser was used for the Raman experiments, with an exposure time of 10 seconds and a 50 × objective lens to focus during measurements. Figure 20 shows the Raman spectra obtained for the transferred graphene and the bare AlGaN NW surface. Compared to the bare AlGaN NW surface, the graphene spectrum shows all the characteristic peaks of graphene at 1340 cm^{-1}, 1583 cm^{-1}, 1620 cm^{-1}, 2675 cm^{-1}, which are often referred as the D, G, D', and 2D-peak, respectively [64], [81]. This confirms the successful transfer of graphene to the AlGaN NW top surface.

In addition, the intensity ratio I_{2D}/I_G is around 2, indicating that the transferred graphene is monolayer in nature [59], [94]. Another indication of successfully obtaining monolayer graphene is by looking at the FWHM of the 2D-peak. Literature reports values between 24-30 cm^{-1} for the FWHM of the 2D-peak for single-layer graphene, and the measured FWHM in Figure 20 is 33.6 cm^{-1}, thus, proving the monolayer nature of the transferred graphene [94].

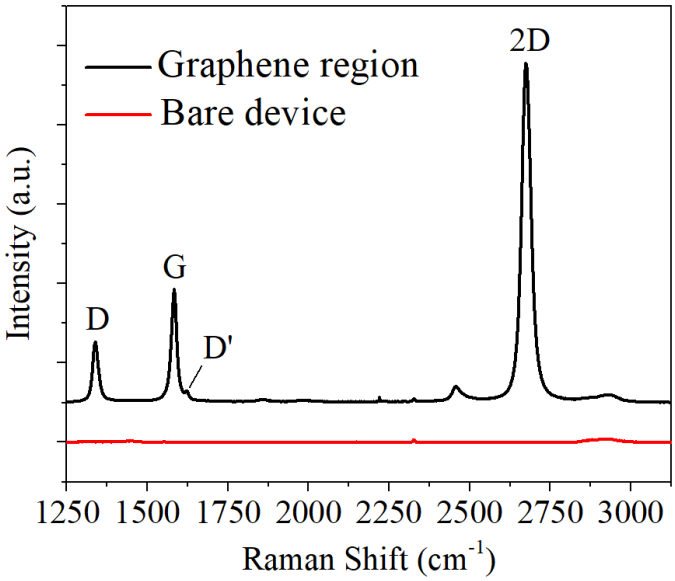

Figure 20: Raman spectra of transferred graphene and bare AlGaN NW surface.

4.4 Characterization of AlGaN NW deep-UV LEDs with transferred graphene electrode

To measure the performance of the device, optical testing was carried out. The electrical injection was realized by a continuous-wave (CW) current source using a Keithley 2400 source meter. The light emission was captured by an optical fiber, which was coupled to a deep-UV spectrometer. Figure 21(a) shows the probe station setup used for optical and electrical measurements. Colloidal Ag paste was applied to the bottom of the n-Si substrate (back electrode). Tungsten probe tips were used to make direct contact to the graphene top electrode. Figure 21(b) shows the EL spectra of the AlGaN NW deep-UV LED devices with the transferred graphene electrode under different injection currents from 5 µA to 150 µA, revealing an emission peak at 280 nm, and increased intensity as the injection current increases.

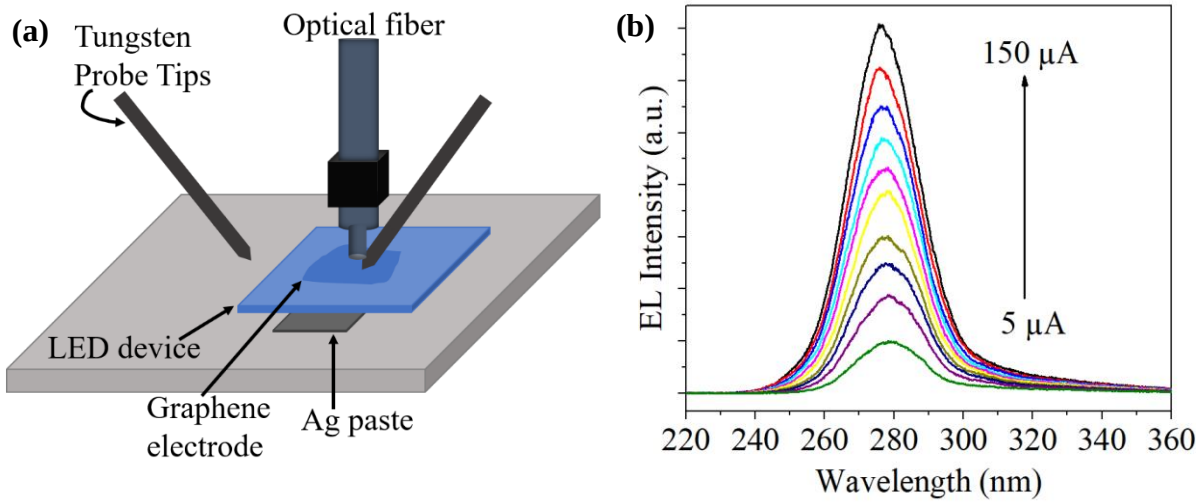

Figure 21: (a) Probe station setup for electrical and optical measurements. (b) EL spectra of AlGaN NW deep-UV LEDs with the transferred graphene electrode under varying injection currents.

Using Figure 21(b), the EL intensity, linewidth (FWHM) and peak wavelength properties were further analysed. Figure 22(a) shows a non-linear increase in the integrated intensity with injection current, with a slight blueshift in peak wavelength seen with increasing injection

current in Figure 22(b), which is consistent with previously reported results [22], [95]. The blueshift is due to the electrostatic screening of the electric polarization field as a result of the carrier density increase, which has been observed previously in the AlGaN UV LEDs with conventional metal electrode [22], [96].

Also shown in Figure 22(a) is an optical image of the light emission. A dim light is visible by eyes. These results therefore suggest that, even though the shape of the transferred graphene is irregular with visible cracks, such transferred graphene can act as a suitable conductive layer for the AlGaN NW deep-UV LEDs, and moreover, graphene does not affect the inherent characteristics of these devices.

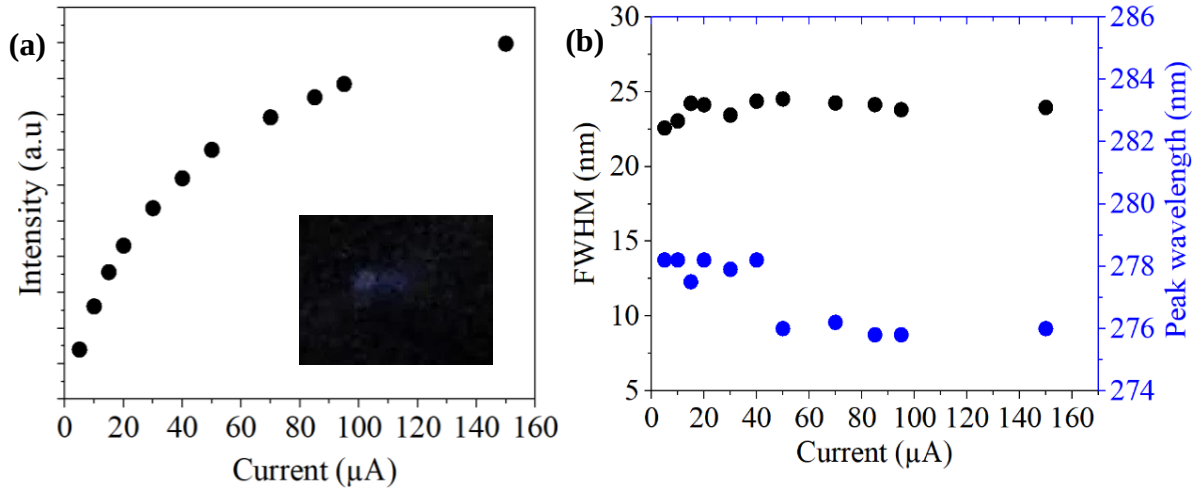

Figure 22: (a) EL intensity versus injection current, with inset showing a photo of the light emission from AlGaN NW deep-UV LEDs with the transferred graphene electrode. (b) FWHM and peak wavelength versus injection current.

Chapter 5: AlGaN NW deep-UV LEDs with patterned graphene electrodes

In this chapter, the fabrication and characterization of AlGaN NW deep-UV LEDs with patterned graphene electrode will be discussed. Different from the graphene used in Chapter 4, graphene on Cu foil is used here in the transfer process. This is followed by standard photolithography process and graphene etching to obtain graphene top electrode with a defined shape and different sizes [97].

5.1 Graphene electrode patterning

Monolayer graphene from Sigma Aldrich was used. The graphene is sandwiched between an 18 μm Cu foil and a thin layer of polymethyl methacrylate (PMMA). Figure 23 shows the graphene transfer procedure [97]. First, the Cu/graphene/PMMA stack was submerged in a chloride-based copper etchant (CE-200 from Sigma Aldrich) at 40 °C for 30 minutes, which helped etch the Cu film. This led to the graphene/PMMA film floating in the Cu etchant, which was then rinsed in a DI water bath to remove etchant residues. Next, the AlGaN NW device structures were introduced to the DI water bath at a tilted angle of 45°, and the graphene/PMMA layer was scooped from the DI water. After the transfer step, the NW/graphene/PMMA device was air-dried for 30 minutes, followed by annealing at 95 °C for 1 hour. Finally, the PMMA was removed by dipping the NW/graphene/PMMA in acetone for 30 minutes, followed by washing with IPA and DI water, and dried by N_2 gas.

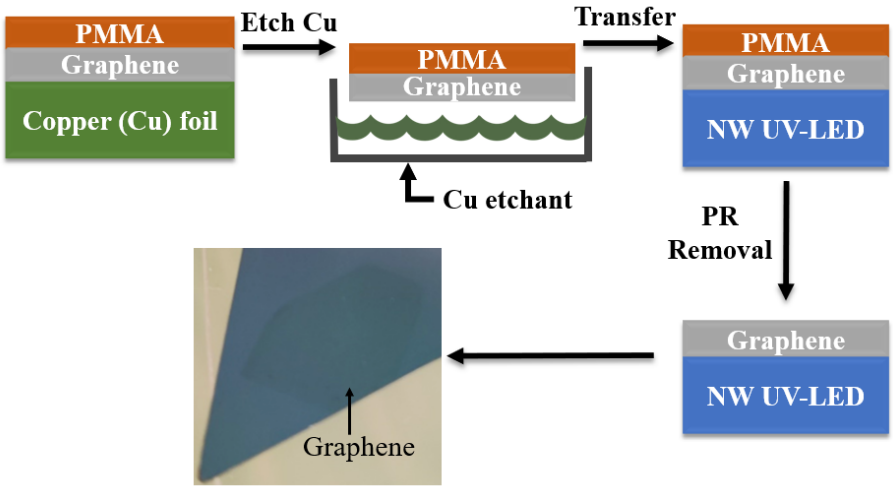

Figure 23: Process flow of graphene transfer to AlGaN NW device structures using graphene on Cu foil [97].

To pattern the graphene electrode, standard lithography was used, as shown in Figure 24 [97]. After graphene transfer, the NW/graphene device was coated with 1.4 µm photoresist (S1813) using a Laurell spin coater, followed by baking at 115 °C for 1 minute. Next, UV exposure at a dose of 130 mJ/cm^2 was carried out with an EVG 620 aligner, using the appropriate mask. The device was developed using MF-319 developer for 1 minute, which was accompanied by DI water rinsing. Next, the exposed graphene was etched using reactive ion etching (RIE) for 90 seconds using O_2 gas, with a flow rate of 48 sccm and RF power of 100 W. Lastly, the photoresist was removed using warm acetone, IPA, and DI water, followed by N_2 drying. Graphene electrodes with dimensions of 1 × 1, 0.5 × 0.5 and 0.3 × 0.3 mm^2 were successfully fabricated in the end.

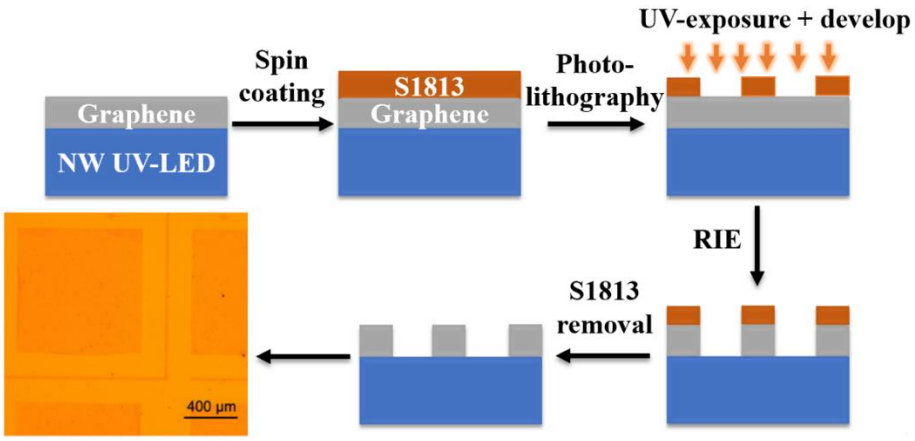

Figure 24: Process flow for the fabrication of graphene electrode with different sizes after graphene transfer [97].

5.2 Characterization of AlGaN NW deep-UV LEDs with patterned graphene electrodes

To measure the device characteristics, optical and electrical testing were carried out. Figure 25 shows the EL spectra of the AlGaN NW deep-UV LEDs with the patterned graphene electrode at injection currents from 10 µA to 480 µA; light emission peak at 248 nm can be seen.

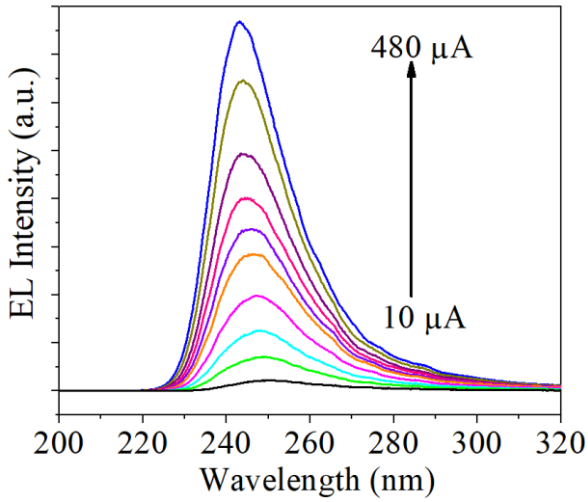

Figure 25: EL spectra of AlGaN NW deep-UV LEDs with the transferred graphene electrode under varying injection currents.

Figure 26(a) and Figure 26(b) show EL intensity, FWHM, and peak position versus injection current. Overall, similar EL characteristics compared with the 280 nm emitting devices (described earlier in Chapter 4) can be seen; except that quantum-confined Stark effect is more noticeable for devices emitting at 240 nm. The inset of Figure 26(a) shows a bright light emission from the AlGaN NW devices with patterned graphene electrode (1 mm × 1 mm), and the light emission region is consistent with the shape of the fabricated electrode.

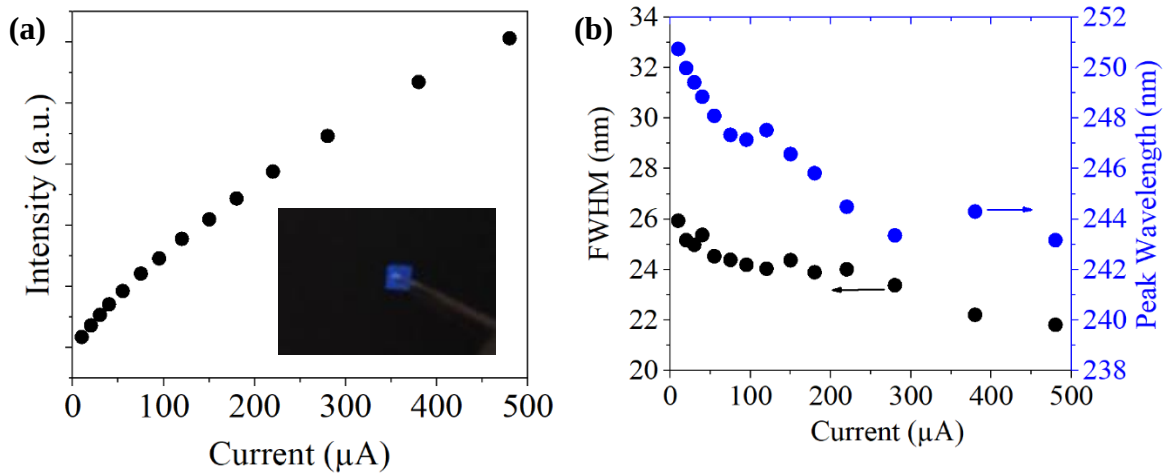

Figure 26: (a) EL intensity versus injection current with inset showing light emission from AlGaN NW deep-UV LEDs with patterned graphene electrode. (b) FWHM and peak wavelength versus injection current.

5.3. Performance comparison of devices with graphene electrode and metal electrode

This section compares the performance of the devices with patterned graphene electrodes to the devices having conventional metal electrodes at 240 nm. Comparison was made using light output power, EQE, and I-V curves, measured from 1 × 1 mm^2 devices. Thin metal bilayers were fabricated using photolithography and metallization techniques on top of the NW surface, consisting of 7 nm Ti and 7 nm Au [22], [23].

5.3.1. Light output power and EQE comparison

Figure 27(a) shows the light output with increasing injection current for the devices with graphene electrode and metal electrode [97]. At small injection currents, i.e., below 0.2 mA, the light output power of the devices with graphene electrode is significantly higher than that of the devices with metal electrode. The light output of the AlGaN NW deep-UV LEDs increases by approximately two folds using the graphene electrode. However, the light output for the devices with graphene electrode tends to saturate as the injection current increases, compared to devices with metal electrode. This saturation gives an indication for an efficiency droop phenomenon for devices with graphene electrode [97].

To further investigate efficiency droop, relative EQE was estimated from the light output power for devices with graphene and metal electrodes. The relative EQE was estimated by taking the ratio of the light output power to the injected current. For comparison purposes, both devices were measured in the same setup. EQE plot for the devices with graphene electrodes and metal electrodes are shown in Figure 27(b), with increasing injection current ranging from 0.01 mA to 0.5 mA [97]. It is seen that the EQE of the devices with graphene electrode are higher than the EQE of the devices with metal electrode at low injection currents. Nonetheless, a more severe efficiency droop is seen in devices with graphene electrode, with an earlier onset of the droop at lower injection currents when compared to the devices with metal electrode. The arrow indicates the onset of efficiency droop for the metal electrode devices.

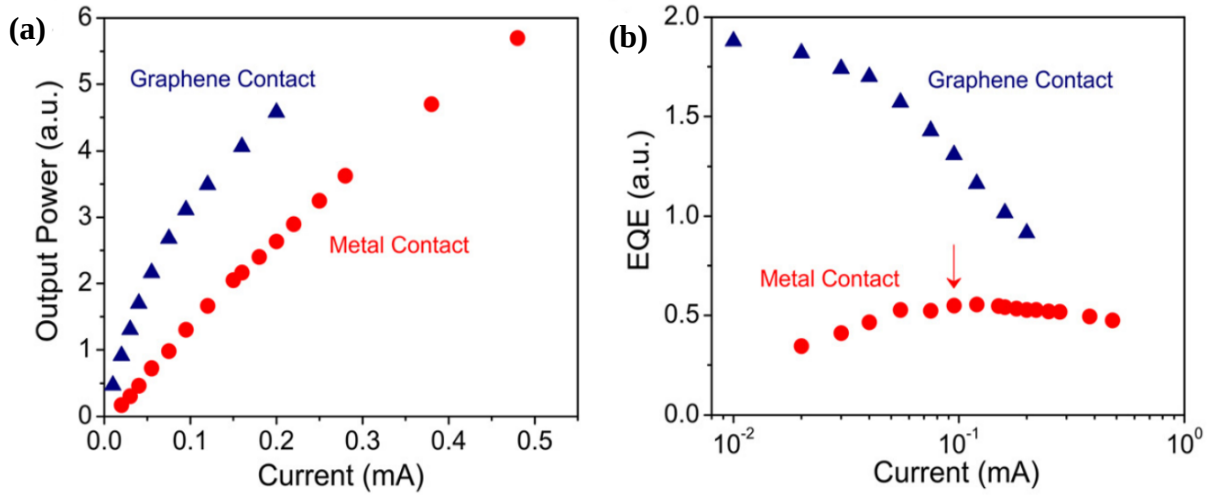

Figure 27: Comparison of devices with graphene electrode to devices with metal electrode. (a) Light output power versus injection current. (b) EQE versus injection current [97].

5.3.2. I-V curve comparison

Figure 28 compares the I-V curves in semi-logarithmic scale for devices with graphene electrode and metal electrode [97]. The I-V characteristics of devices with graphene electrode are worse compared to devices with metal electrode. Series resistance for both cases was calculated using the slope of the I-V curve at approximately 10 V. The estimated values for devices with metal electrode and graphene electrode were 430 Ω and 29 kΩ, respectively. High series resistance for devices with graphene electrode leads to a significant heating effect, which can be the primary cause for the severe efficiency droop.

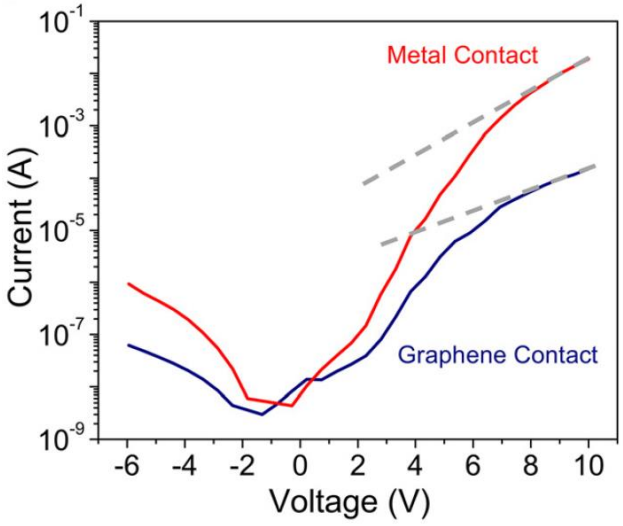

Figure 28: I-V characteristics of devices with metal and graphene electrode [97].

Chapter 6: Discussions

This section provides further discussions on devices with graphene electrode, such as the possible cause for the large series resistance seen earlier, graphene degradation, and graphene transfer challenges.

6.1. Possible mechanism for large series resistance and limitations of devices with graphene electrode

This section discusses the possible reasons for the large series resistance derived for devices with graphene electrode. As a starting point, SEM images of as-grown AlGaN NWs were studied. A typical SEM image is shown in Figure 29, taken at a 45° tilting angle [97]. The NWs are densely packed and relatively uniform overall.

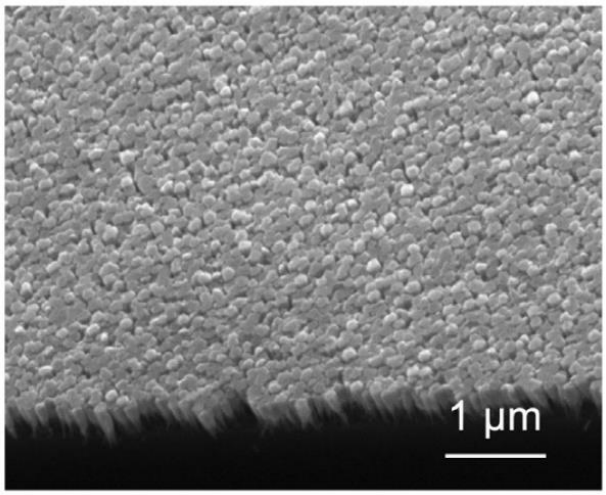

Figure 29: SEM of the as-grown NW wafer at a tilting angle of 45° [97].

Although the NWs look relatively uniform, there is a size distribution. Figure 30 depicts the variations in height and diameter for the as-grown AlGaN NWs analysed by ImageJ [97]. The mean and standard deviation for the NW length (height distribution) are 452 nm and 39 nm,

respectively. For the NW top facet, the mean and standard deviation for the diameter are 115 nm and 13 nm, respectively. Thus, it is evident that variations exist in the NW dimensions, with a more severe variation seen for the NW length, compared with the NW diameter. It can be rationalized that due to the existing height variations, uneven NW height is obtained, which consequently leads to non-uniform graphene electrode on the NW top surface, leading to large contact resistance, which contributes to the large series resistance.

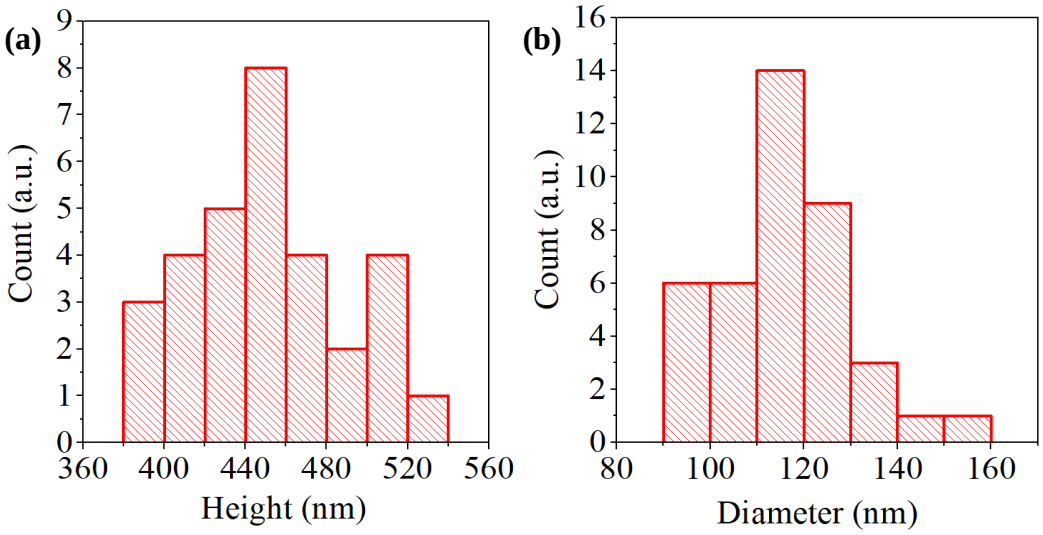

Figure 30: Statistics for the as-grown NWs showing (a) height distribution and (b) NW top facet diameter distribution [97].

Figure 31 shows the SEM of the fabricated graphene electrode on the AlGaN NW top surface [97]. Figure 31(a) shows the graphene surface at a smaller magnification, which shows features like cracks and wrinkles (marked by arrows), indicating the non-uniform nature of the transferred graphene. Figure 31(b) shows the same graphene surface at a higher magnification, showing the wrinkles more clearly. It can also be seen that the taller NWs (compared to the adjacent NWs) are piercing the graphene surface. It is evident that the uneven nature of graphene transfer due to NW height variation leads to defects like cracks and wrinkles on the graphene surface, which subsequently results in poor adhesion of graphene on the NW top

surface, as well as the large sheet resistance of graphene itself, causing large contact resistance. Previous studies have shown similar effects, as described earlier in Chapter 2. Nonetheless, this issue can be potentially addressed by NWs grown by SAG.

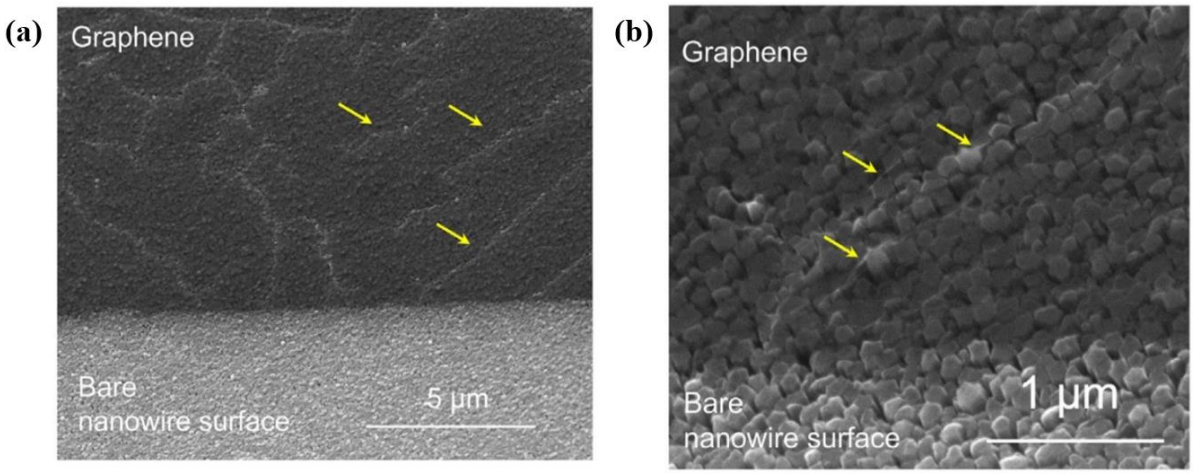

Figure 31: SEM images of transferred graphene on AlGaN NWs at (a) small scale, (b) large scale [97].

Raman spectroscopy was performed on devices with patterned graphene electrodes to further confirm the non-uniform nature of the graphene electrode. Raman spectra were collected on various regions of the device, and two such regions with transferred graphene (labelled #1 and #2) are shown in Figure 32, along with a comparison with the bare AlGaN NW surface [97]. It was observed that for different regions of the device, even though the same characteristic peaks are visible (D-, G- and 2D-peak) for graphene, the intensity ratio of the 2D- and G-peak (i.e., I_{2D}/I_G) differ. The observed variation for the intensity peaks on different parts of the graphene electrode is another indication of non-uniformity [68], [98].

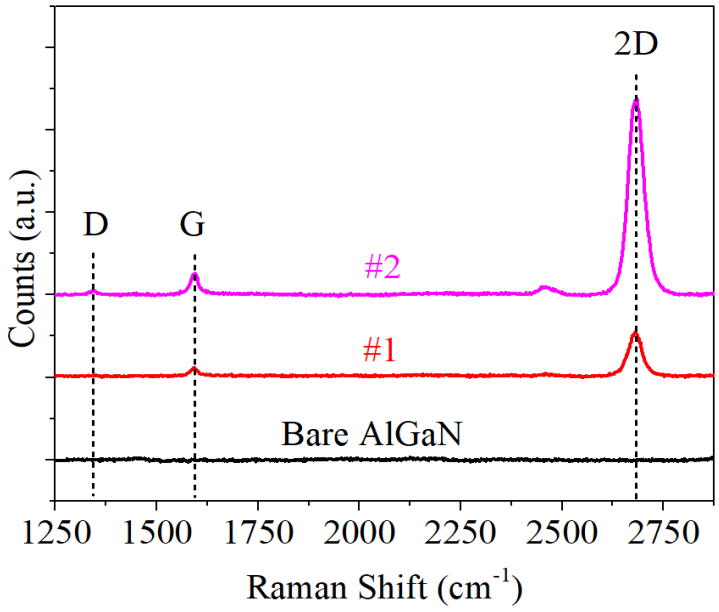

Figure 32: Raman spectra of devices with graphene electrode and bare AlGaN NW surface showing graphene characteristic peaks, where "#1" and "#2" refer to the spectra measured from two different graphene regions on the same electrode [97].

Lastly, it is worth noting that, for the present devices with graphene electrode, the top contact is n-GaN, the work function of which is similar to that of pristine graphene. As such, the work function difference might not be the main cause for the large contact resistance.

6.2. Graphene degradation analysis using Raman spectroscopy

Previous reports have shown graphene damage after continuous electrical injection. Kim et al. have reported that under a continuous current injection, the luminescent region became smaller, and current levels were seen to reduce after 30 seconds of continuous biasing [28]. This was attributed to the high junction temperature and joule heating at high injection currents, which facilitated the formation of CO and CO_2 as a result of the interaction of C-C from the graphene with O_2 in the air [29], [99]. Kim et al. further reported a decrease in the I_G/I_{2D} intensity ratio after continuous electrical injection from the Raman spectra of their FLG. The

change in the intensity ratio was attributed to the thinning of their graphene film, leading to degradation of graphene and consequently, effecting overall device performance [28]. Another possible indication of graphene degradation from Raman spectra is the intensity of the D- and D'-peaks at 1340 cm^{-1} and 1620 cm^{-1} respectively [64], [81].

In this study, Raman measurements were performed on the devices with graphene electrode before and after electrical injection to examine the degradation of the transferred graphene. The Raman spectra are shown in Figure 33. No change in the intensity can be seen after electrical injection. However, due to the uneven and non-uniform nature of the transferred graphene, no conclusions can be made about the degradation of graphene in this study (e.g., strain in graphene from nonuniform NW height can also affect the I_{2D}/I_G peak ratio).

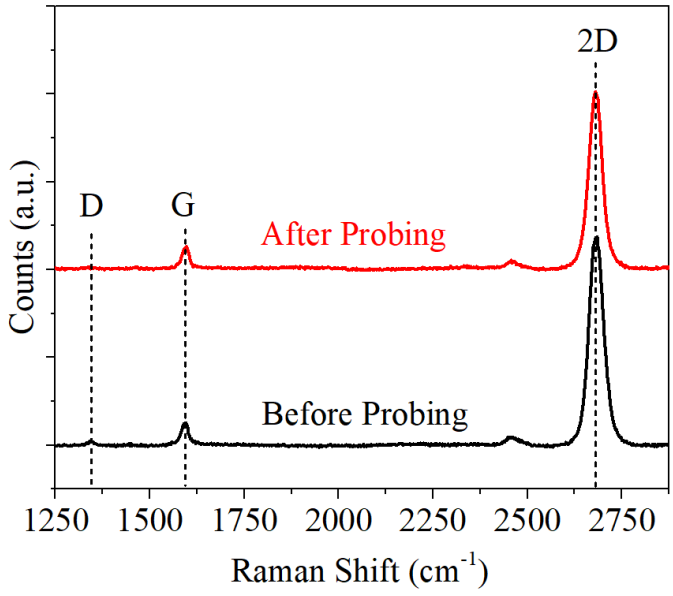

Figure 33: Raman spectra of devices with graphene electrode, before and after electrical injection.

6.3. Graphene transfer challenges: Easy Transfer graphene versus Cu foil graphene

Hitherto, poor graphene adhesion due to variation in as-grown NW height has been discussed, however, graphene adhesion issues also potentially arise from inefficient graphene

transfer [100]–[102]. Inefficient graphene transfer can occur due to delamination from the growth substrate, or from the removal of the SL employed, as shown in Figure 34 [100]. In this thesis, two different growth substrates (polymer and Cu foil) were used, however, the same SL (PMMA) was used for both transfers.

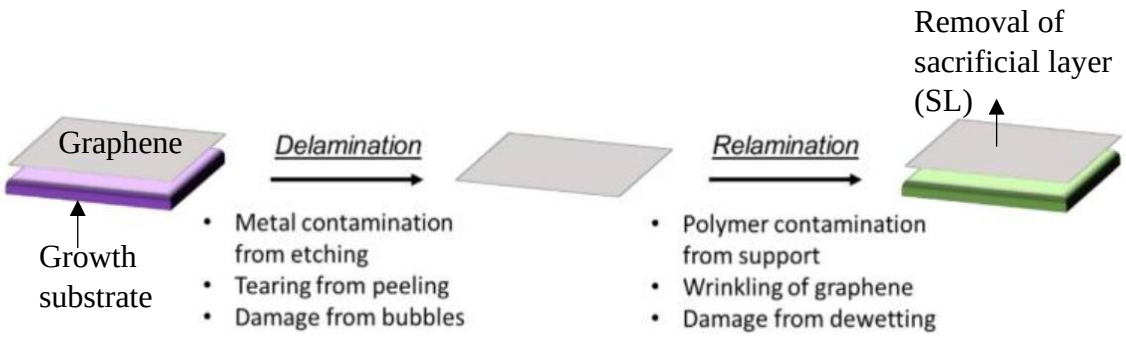

Figure 34: Graphene transfer challenges during delamination from growth substate and re-lamination on desired substrate, accompanied by common issues arising at each step [100].

Chapter 4 and Chapter 5 discuss graphene transfer process with two growth substrates, polymer film (Easy Transfer graphene) and graphene on Cu foil, respectively. Comparing Figure 35(a) and Figure 35(b), a visible difference can be seen in the quality of transferred graphene. Easy Transfer graphene yielded transferred graphene with several cracks, whereas the graphene on Cu foil yielded a more uniform graphene transfer. Easy transfer graphene makes use of a water-soluble polymer substrate which is detached from the graphene/SL stack by immersing in DI water. On the other hand, for graphene on Cu foil transfer, the Cu foil has to be etched by an appropriate etchant to detach from the graphene/PMMA stack.

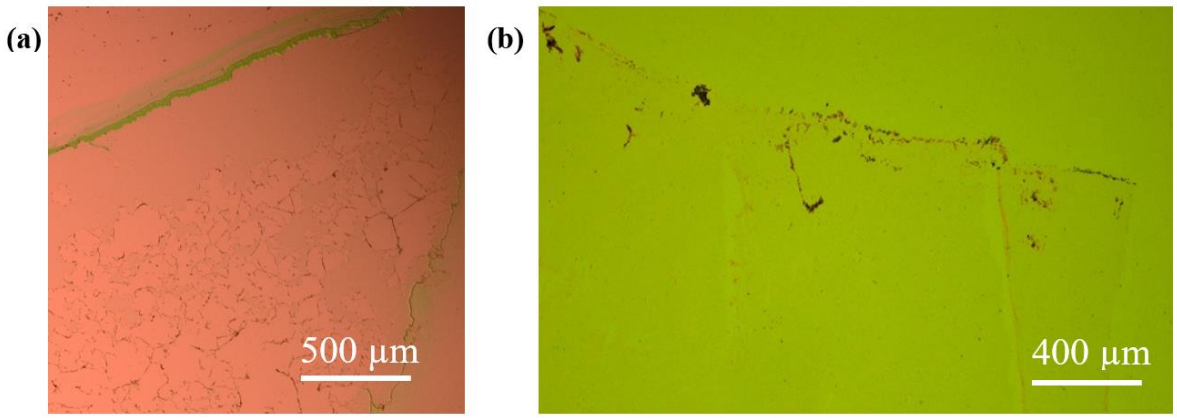

Figure 35: Graphene transfer to AlGaN NW device structures using (a) Easy Transfer graphene, (b) graphene on Cu foil.

Even though both types of substrates, i.e., metal (Cu) and polymer, have their pros and cons, detachment of graphene from polymeric material is the primary reason for wrinkles and cracks. Literature reports several studies where the removal of the polymer SL (specifically PMMA) causes defects in graphene like cracks, wrinkles and residues [100]–[104]. Alternate materials to PMMA as SL have been explored like paraffin wax, which has a higher thermal expansion coefficient and lower chemical reactivity, eliminating the residue and wrinkle issues associated with PMMA [105], [106]. The same reasoning can be applied in this study for Easy transfer graphene, as the polymer used in Chapter 4 serves the dual purpose of a substrate and a SL, causing uneven transfer of graphene due to detachment from a polymer layer at both the delamination stage and the re-lamination stage of the graphene transfer process. For future graphene transfers, graphene on Cu foil will be used. However, as seen from the SEM image in Figure 31, the Cu film graphene also suffers from cracks (which was exacerbated by the uneven NW height), as PMMA is still employed as a SL. Thus, there is scope for further improving the graphene transfer process.

Chapter 7: Conclusion and future work

This thesis successful demonstrated surface-emitting vertically injected AlGaN NW deep-UV LEDs with transferred monolayer graphene as the top electrode from 240 to 280 nm. The graphene transfer was confirmed by Raman spectroscopy and XPS experiments. Bright light emission was measured from devices with patterned graphene electrodes. EL studies show an expected increase in EL intensity as injection current increases, along with a blueshift of the peak wavelength and spectral narrowing of the linewidth, which are common characteristics of such AlGaN NW deep-UV LEDs.

Moreover, a detailed comparison was presented of devices with patterned graphene electrode and devices with patterned conventional metal electrodes. Light output power of the devices with graphene electrode was observed to be higher than that of the devices with metal electrodes, however, the output power for the graphene electrode devices began to saturate, indicating efficiency droop. The EQE plot showed an earlier onset of efficiency droop, i.e., at a smaller injection current for devices with graphene electrode. Furthermore, the I-V characteristics of the graphene electrode devices were worse than that of the metal electrode devices, with a very high series resistance of 29 kΩ, which explained the earlier onset of efficiency droop for the devices with graphene electrode. SEM images showed cracked, wrinkled, and pierced graphene on the AlGaN NW top surface, leading to poor adhesion of graphene due to uneven NW height, contributing to efficiency droop and high contact resistance. Raman spectroscopy confirmed the non-uniform nature of graphene transfer as the I_{2D}/I_G intensity ratios varied on different parts of the device.

The findings in this thesis indicate that graphene can help improve the optical performance of short-wavelength surface-emitting vertical AlGaN NW LEDs, the very first demonstration of its kind at emission wavelengths shorter than 280 nm without metal electrodes. However,

further development of these devices requires overcoming certain challenges. Future work will focus on resolving the earlier onset of efficiency droop for devices with graphene electrode by decreasing the contact resistance between graphene and the NW top surface. This can be achieved in two ways: more uniform growth of NWs and by improving the graphene transfer process. More uniform growth of NWs can be realized by SAG on Si, which helps produce NWs with the same height [107]. In addition, improvement of the graphene transfer process by finding alternate materials to the polymer SL will also help in more uniform graphene transfer. Furthermore, using MLG or FLG instead of monolayer graphene can be a potential solution for the high series resistance of 29 kΩ. Studies have shown a reduction of sheet resistance from 660 Ω/sq for transferred monolayer graphene to less than 220 Ω/sq for transferred FLG in GaN-based LEDs [82]. However, as the thickness of graphene layer increases, the transparency of the material decreases. Lastly, to achieve better contact, future steps will also include depositing metal grids on the AlGaN NW UV-LEDs after the transfer of graphene electrodes.

References

[1] S. Vilhunen, H. Särkkä, and M. Sillanpää, "Ultraviolet light-emitting diodes in water disinfection," *Environ. Sci. Pollut. Res. Int.*, vol. 16, no. 4, pp. 439–442, Jun. 2009, doi: 10.1007/s11356-009-0103-y.

[2] W. Kowalski, "Ultraviolet Germicidal Irradiation Handbook," 2009, pp. 17–50. doi: 10.1007/978-3-642-01999-9_2.

[3] J. Mellqvist and A. Rosén, "DOAS for flue gas monitoring—I. Temperature effects in the U.V./visible absorption spectra of NO, NO2, SO2 and NH3," *J. Quant. Spectrosc. Radiat. Transf.*, vol. 56, no. 2, pp. 187–208, Aug. 1996, doi: 10.1016/0022-4073(96)00042-8.

[4] C. for D. and R. Health, "UV Lights and Lamps: Ultraviolet-C Radiation, Disinfection, and Coronavirus," *FDA*, Feb. 2021, Accessed: Jun. 15, 2022. [Online]. Available: https://www.fda.gov/medical-devices/coronavirus-covid-19-and-medical-devices/uv-lights-and-lamps-ultraviolet-c-radiation-disinfection-and-coronavirus

[5] M. Kneissl, "A Brief Review of III-Nitride UV Emitter Technologies and Their Applications," in *III-Nitride Ultraviolet Emitters: Technology and Applications*, M. Kneissl and J. Rass, Eds. Cham: Springer International Publishing, 2016, pp. 1–25. doi: 10.1007/978-3-319-24100-5_1.

[6] R. M. Biefeld, M. H. Crawford, J. Han, S. R. Lee, G. A. Petersen, and A. F. Wright, "The Band Gap of AlGaN Alloys," *Appl. Phys. Lett.*, Art. no. SAND99-0274J, Jan. 1999, Accessed: May 24, 2022. [Online]. Available: https://www.osti.gov/biblio/3336-band-gap-algan-alloys

[7] Zetian Mi and Chennupati Jagadish, *III-Nitride Semiconductor Optoelectronics*, no. volume 96. Cambridge, MA: Academic Press, 2017. Accessed: Jun. 05, 2022. [Online]. Available: https://proxy.library.mcgill.ca/login?url=https://search.ebscohost.com/login.aspx?direct=true&db=nlebk&AN=1158641&scope=site

[8] Z. Gong, M. Gaevski, V. Adivarahan, W. Sun, M. Shatalov, and M. Asif Khan, "Optical power degradation mechanisms in AlGaN-based 280nm deep ultraviolet light-emitting diodes on sapphire," *Appl. Phys. Lett.*, vol. 88, no. 12, p. 121106, Mar. 2006, doi: 10.1063/1.2187429.

[9] I. Yu. Evstratov, V. F. Mymrin, S. Yu. Karpov, and Yu. N. Makarov, "Current crowding effects on blue LED operation," *Phys. Status Solidi C*, vol. 3, no. 6, pp. 1645–1648, 2006, doi: 10.1002/pssc.200565417.

[10] H. Kim *et al.*, “Design of high-efficiency GaN-based light emitting diodes with vertical injection geometry,” *Appl. Phys. Lett.*, vol. 91, no. 2, p. 023510, Jul. 2007, doi: 10.1063/1.2756139.

[11] V. Adivarahan *et al.*, “Vertical Injection Thin Film Deep Ultraviolet Light Emitting Diodes with AlGaN Multiple-Quantum Wells Active Region,” *Appl. Phys. Express*, vol. 2, no. 9, p. 092102, Sep. 2009, doi: 10.1143/APEX.2.092102.

[12] L. Zhou *et al.*, “Vertical injection thin-film AlGaN/AlGaN multiple-quantum-well deep ultraviolet light-emitting diodes,” *Appl. Phys. Lett.*, vol. 89, no. 24, p. 241113, Dec. 2006, doi: 10.1063/1.2408643.

[13] Y. J. Sung, D.-W. Kim, G. Y. Yeom, and K. S. Kim, “Performance of vertical type deep UV light-emitting diodes depending on the Ga-face n-contact hole density,” *Appl. Phys. Lett.*, vol. 118, no. 23, p. 231102, Jun. 2021, doi: 10.1063/5.0052416.

[14] M. Takeuchi, T. Maegawa, H. Shimizu, S. Ooishi, T. Ohtsuka, and Y. Aoyagi, “AlN/AlGaN short-period superlattice sacrificial layers in laser lift-off for vertical-type AlGaN-based deep ultraviolet light emitting diodes,” *Appl. Phys. Lett.*, vol. 94, no. 6, p. 061117, Feb. 2009, doi: 10.1063/1.3081060.

[15] K. B. Nam, J. Li, M. L. Nakarmi, J. Y. Lin, and H. X. Jiang, “Unique optical properties of AlGaN alloys and related ultraviolet emitters,” *Appl. Phys. Lett.*, vol. 84, no. 25, pp. 5264–5266, Jun. 2004, doi: 10.1063/1.1765208.

[16] T. D. Moustakas and R. Paiella, “Optoelectronic device physics and technology of nitride semiconductors from the UV to the terahertz,” *Rep. Prog. Phys.*, vol. 80, no. 10, p. 106501, Sep. 2017, doi: 10.1088/1361-6633/aa7bb2.

[17] F. Glas, “Critical dimensions for the plastic relaxation of strained axial heterostructures in free-standing nanowires,” *Phys. Rev. B*, vol. 74, no. 12, p. 121302, Sep. 2006, doi: 10.1103/PhysRevB.74.121302.

[18] A. Liudi Mulyo *et al.*, “Graphene-Based Transparent Conducting Substrates for GaN/AlGaN Nanocolumn Flip-Chip Ultraviolet Light-Emitting Diodes,” *ACS Appl. Nano Mater.*, vol. 4, no. 9, pp. 9653–9664, Sep. 2021, doi: 10.1021/acsanm.1c02050.

[19] K. Kishino and S. Ishizawa, “Selective-area growth of GaN nanocolumns on Si(111) substrates for application to nanocolumn emitters with systematic analysis of dislocation filtering effect of nanocolumns,” *Nanotechnology*, vol. 26, no. 22, p. 225602, May 2015, doi: 10.1088/0957-4484/26/22/225602.

[20] B. J. May, A. T. M. G. Sarwar, and R. C. Myers, “Nanowire LEDs grown directly on flexible metal foil,” *Appl. Phys. Lett.*, vol. 108, no. 14, p. 141103, Apr. 2016, doi: 10.1063/1.4945419.

[21] S. Zhao, M. Djavid, and Z. Mi, “Surface Emitting, High Efficiency Near-Vacuum Ultraviolet Light Source with Aluminum Nitride Nanowires Monolithically Grown on Silicon,” *Nano Lett.*, vol. 15, no. 10, pp. 7006–7009, Oct. 2015, doi: 10.1021/acs.nanolett.5b03040.

[22] S. Zhao, S. M. Sadaf, S. Vanka, Y. Wang, R. Rashid, and Z. Mi, “Sub-milliwatt AlGaN nanowire tunnel junction deep ultraviolet light emitting diodes on silicon operating at 242 nm,” *Appl. Phys. Lett.*, vol. 109, no. 20, p. 201106, Nov. 2016, doi: 10.1063/1.4967837.

[23] S. M. Sadaf *et al.*, “An AlGaN Core–Shell Tunnel Junction Nanowire Light-Emitting Diode Operating in the Ultraviolet-C Band,” *Nano Lett.*, vol. 17, no. 2, pp. 1212–1218, Feb. 2017, doi: 10.1021/acs.nanolett.6b05002.

[24] D.-S. Leem *et al.*, “High transparency of Ag⁄Zn–Ni solid–solution ohmic contacts for GaN-based ultraviolet light-emitting diodes,” *Appl. Phys. Lett.*, vol. 86, no. 10, p. 102102, Mar. 2005, doi: 10.1063/1.1879084.

[25] W. Hou, C. Stark, S. You, L. Zhao, T. Detchprohm, and C. Wetzel, “Evaluation of metal/indium-tin-oxide for transparent low-resistance contacts to p-type GaN,” *Appl. Opt.*, vol. 51, no. 23, pp. 5596–5600, Aug. 2012, doi: 10.1364/AO.51.005596.

[26] L. Wang *et al.*, “Graphene-based transparent conductive electrodes for GaN-based light emitting diodes: Challenges and countermeasures,” 2015, doi: 10.1016/J.NANOEN.2014.12.035.

[27] Z. Li *et al.*, “The fabrication of GaN-based nanorod light-emitting diodes with multilayer graphene transparent electrodes,” *J. Appl. Phys.*, vol. 113, no. 23, p. 234302, Jun. 2013, doi: 10.1063/1.4811224.

[28] B.-J. Kim *et al.*, “Buried graphene electrodes on GaN-based ultra-violet light-emitting diodes,” *Appl. Phys. Lett.*, vol. 101, no. 3, p. 031108, Jul. 2012, doi: 10.1063/1.4733981.

[29] B.-J. Kim *et al.*, “Large-area transparent conductive few-layer graphene electrode in GaN-based ultra-violet light-emitting diodes,” *Appl. Phys. Lett.*, vol. 99, no. 14, p. 143101, Oct. 2011, doi: 10.1063/1.3644496.

[30] B.-J. Kim *et al.*, “GaN-based ultraviolet light-emitting diodes with AuCl3-doped graphene electrodes,” *Opt. Express*, vol. 21, pp. 29025–30, Nov. 2013, doi: 10.1364/OE.21.029025.

[31] G. Jo *et al.*, “Large-scale patterned multi-layer graphene films as transparent conducting electrodes for GaN light-emitting diodes,” *Nanotechnology*, vol. 21, no. 17, p. 175201, Apr. 2010, doi: 10.1088/0957-4484/21/17/175201.

[32] A. V. Babichev *et al.*, “GaN nanowire ultraviolet photodetector with a graphene transparent contact,” *Appl. Phys. Lett.*, vol. 103, no. 20, p. 201103, Nov. 2013, doi: 10.1063/1.4829756.

[33] T. Hoon Seo *et al.*, “Graphene-silver nanowire hybrid structure as a transparent and current spreading electrode in ultraviolet light emitting diodes,” *Appl. Phys. Lett.*, vol. 103, no. 5, p. 051105, Jul. 2013, doi: 10.1063/1.4817256.

[34] J. H. Warner, F. Schaffel, M. Rummeli, and A. Bachmatiuk, *Graphene: Fundamentals and emergent applications*. Newnes, 2012.

[35] Y. Y. Zhang and Y. T. Gu, “Mechanical properties of graphene: Effects of layer number, temperature and isotope,” *Comput. Mater. Sci.*, vol. 71, pp. 197–200, Apr. 2013, doi: 10.1016/j.commatsci.2013.01.032.

[36] M. Junaid *et al.*, “A Review on Graphene-Based Light Emitting Functional Devices,” *Molecules*, vol. 25, no. 18, Art. no. 18, Jan. 2020, doi: 10.3390/molecules25184217.

[37] J.-H. Chen, C. Jang, S. Xiao, M. Ishigami, and M. S. Fuhrer, “Intrinsic and extrinsic performance limits of graphene devices on SiO2,” *Nat. Nanotechnol.*, vol. 3, no. 4, Art. no. 4, Apr. 2008, doi: 10.1038/nnano.2008.58.

[38] Y. Song, W. Fang, R. Brenes, and J. Kong, “Challenges and opportunities for graphene as transparent conductors in optoelectronics,” *Nano Today*, vol. 10, no. 6, pp. 681–700, Dec. 2015, doi: 10.1016/j.nantod.2015.11.005.

[39] R. R. Nair *et al.*, “Fine structure constant defines visual transparency of graphene,” *Science*, vol. 320, no. 5881, p. 1308, Jun. 2008, doi: 10.1126/science.1156965.

[40] C. Zhao *et al.*, “III-nitride nanowires on unconventional substrates: From materials to optoelectronic device applications,” *Prog. Quantum Electron.*, vol. 61, pp. 1–31, Sep. 2018, doi: 10.1016/j.pquantelec.2018.07.001.

[41] R. Jiang and X. Meng, “The characterization of AlGaN nanowires prepared via chemical vapor deposition,” *J. Mater. Sci. Mater. Electron.*, vol. 30, no. 17, pp. 16266–16274, Sep. 2019, doi: 10.1007/s10854-019-01997-4.

[42] K. A. Bertness *et al.*, “Catalyst-free growth of GaN nanowires,” *J. Electron. Mater.*, vol. 35, no. 4, pp. 576–580, Apr. 2006, doi: 10.1007/s11664-006-0102-4.

[43] C. He *et al.*, “Growth and Characterization of Ternary AlGaN Alloy Nanocones across the Entire Composition Range,” *ACS Nano*, vol. 5, no. 2, pp. 1291–1296, Feb. 2011, doi: 10.1021/nn1029845.

[44] J. Li, D. Wang, and R. R. LaPierre, *Advances in III-V Semiconductor Nanowires and Nanodevices*. Bentham Science Publishers, 2011.

[45] J. Su *et al.*, “Growth of AlGaN nanowires by metalorganic chemical vapor deposition,” *Appl. Phys. Lett.*, vol. 87, no. 18, p. 183108, Oct. 2005, doi: 10.1063/1.2126113.

[46] Y.-H. Ra, S. Kang, and C.-R. Lee, “Ultraviolet Light-Emitting Diode Using Nonpolar AlGaN Core–Shell Nanowire Heterostructures,” *Adv. Opt. Mater.*, vol. 6, no. 14, p. 1701391, 2018, doi: 10.1002/adom.201701391.

[47] J.-W. Min *et al.*, “Unleashing the potential of molecular beam epitaxy grown AlGaN-based ultraviolet-spectrum nanowires devices,” *J. Nanophotonics*, vol. 12, no. 4, p. 043511, Jul. 2018, doi: 10.1117/1.JNP.12.043511.

[48] H. Sekiguchi, K. Kato, J. Tanaka, A. Kikuchi, and K. Kishino, “Ultraviolet GaN-based nanocolumn light-emitting diodes grown on n-(111) Si substrates by rf-plasma-assisted molecular beam epitaxy,” *Phys. Status Solidi A*, vol. 205, no. 5, pp. 1067–1069, 2008, doi: 10.1002/pssa.200778733.

[49] S. D. Carnevale, T. F. Kent, P. J. Phillips, M. J. Mills, S. Rajan, and R. C. Myers, “Polarization-Induced pn Diodes in Wide-Band-Gap Nanowires with Ultraviolet Electroluminescence,” *Nano Lett.*, vol. 12, no. 2, pp. 915–920, Feb. 2012, doi: 10.1021/nl203982p.

[50] S. D. Carnevale *et al.*, “Mixed Polarity in Polarization-Induced p–n Junction Nanowire Light-Emitting Diodes,” *Nano Lett.*, vol. 13, no. 7, pp. 3029–3035, Jul. 2013, doi: 10.1021/nl400200g.

[51] B. Janjua *et al.*, “Self-planarized quantum-disks-in-nanowires ultraviolet-B emitters utilizing pendeo-epitaxy,” *Nanoscale*, vol. 9, no. 23, pp. 7805–7813, Jun. 2017, doi: 10.1039/C7NR00006E.

[52] M. Belloeil, “Molecular beam epitaxy growth and optical characterization of GaN/AlGaN nanowire heterostructures emitting in the ultraviolet,” 2017.

[53] K. Hestroffer, “Growth and characterization of GaN nanowires and of GaN/AlN nanowire heterostructures,” phdthesis, Université de Grenoble, 2012. Accessed: May 20, 2022. [Online]. Available: https://tel.archives-ouvertes.fr/tel-00863433

[54] A. Pierret, “Propriétés structurales et optiques de nanostructures III-N semiconductrices à grand gap : nanofils d’AlxGa1-xN synthétisés par épitaxie par jets moléculaires et

nanostructures de nitrure de bore.," phdthesis, Université Pierre et Marie Curie - Paris VI, 2013. Accessed: May 20, 2022. [Online]. Available: https://tel.archives-ouvertes.fr/tel-01020119

[55] B. H. Le, S. Zhao, X. Liu, S. Y. Woo, G. A. Botton, and Z. Mi, "Controlled Coalescence of AlGaN Nanowire Arrays: An Architecture for Nearly Dislocation-Free Planar Ultraviolet Photonic Device Applications," *Adv. Mater.*, vol. 28, no. 38, pp. 8446–8454, 2016, doi: 10.1002/adma.201602645.

[56] P. Liu *et al.*, "Emerging trends in 2D nanotechnology that are redefining our understanding of 'Nanocomposites,'" *Nano Today*, vol. 21, May 2018, doi: 10.1016/j.nantod.2018.04.012.

[57] F. Bonaccorso, A. Lombardo, T. Hasan, Z. Sun, L. Colombo, and A. C. Ferrari, "Production and processing of graphene and 2d crystals," *Mater. Today*, vol. 15, no. 12, pp. 564–589, Dec. 2012, doi: 10.1016/S1369-7021(13)70014-2.

[58] J. Yamada *et al.*, "Transfer-free fabrication of a graphene transparent electrode on a GaN-based light-emitting diode using the direct precipitation method," *Jpn. J. Appl. Phys.*, vol. 58, no. 4, p. 040904, Mar. 2019, doi: 10.7567/1347-4065/aafe70.

[59] Y. Hwangbo *et al.*, "Interlayer non-coupled optical properties for determining the number of layers in arbitrarily stacked multilayer graphenes," *Carbon*, vol. 77, pp. 454–461, Oct. 2014, doi: 10.1016/j.carbon.2014.05.050.

[60] V. Kumar, A. Kumar, D.-J. Lee, and S.-S. Park, "Estimation of Number of Graphene Layers Using Different Methods: A Focused Review," *Materials*, vol. 14, no. 16, Art. no. 16, Jan. 2021, doi: 10.3390/ma14164590.

[61] A. C. Ferrari and D. M. Basko, "Raman spectroscopy as a versatile tool for studying the properties of graphene," *Nat. Nanotechnol.*, vol. 8, no. 4, Art. no. 4, Apr. 2013, doi: 10.1038/nnano.2013.46.

[62] L. Chong, H. Guo, Y. Zhang, Y. Hu, and Y. Zhang, "Raman Study of Strain Relaxation from Grain Boundaries in Epitaxial Graphene Grown by Chemical Vapor Deposition on SiC," *Nanomaterials*, vol. 9, no. 3, Art. no. 3, Mar. 2019, doi: 10.3390/nano9030372.

[63] A. Eckmann *et al.*, "Probing the Nature of Defects in Graphene by Raman Spectroscopy," *Nano Lett.*, vol. 12, no. 8, pp. 3925–3930, Aug. 2012, doi: 10.1021/nl300901a.

[64] L. M. Malard, M. A. Pimenta, G. Dresselhaus, and M. S. Dresselhaus, "Raman spectroscopy in graphene," *Phys. Rep.*, vol. 473, no. 5, pp. 51–87, Apr. 2009, doi: 10.1016/j.physrep.2009.02.003.

[65] A. C. Ferrari *et al.*, “Raman Spectrum of Graphene and Graphene Layers,” *Phys. Rev. Lett.*, vol. 97, no. 18, p. 187401, Oct. 2006, doi: 10.1103/PhysRevLett.97.187401.

[66] S. Roscher, R. Hoffmann, and O. Ambacher, “Determination of the graphene–graphite ratio of graphene powder by Raman 2D band symmetry analysis,” *Anal. Methods*, vol. 11, no. 9, pp. 1224–1228, 2019, doi: 10.1039/C8AY02619J.

[67] C. Ferrante *et al.*, “Raman spectroscopy of graphene under ultrafast laser excitation,” *Nat. Commun.*, vol. 9, no. 1, Art. no. 1, Jan. 2018, doi: 10.1038/s41467-017-02508-x.

[68] S. Berciaud, S. Ryu, L. E. Brus, and T. F. Heinz, “Probing the Intrinsic Properties of Exfoliated Graphene: Raman Spectroscopy of Free-Standing Monolayers,” *Nano Lett.*, vol. 9, no. 1, pp. 346–352, Jan. 2009, doi: 10.1021/nl8031444.

[69] A. Reina *et al.*, “Large Area, Few-Layer Graphene Films on Arbitrary Substrates by Chemical Vapor Deposition,” *Nano Lett.*, vol. 9, no. 1, pp. 30–35, Jan. 2009, doi: 10.1021/nl801827v.

[70] J. D. Caldwell *et al.*, “Technique for the Dry Transfer of Epitaxial Graphene onto Arbitrary Substrates,” *ACS Nano*, vol. 4, no. 2, pp. 1108–1114, Feb. 2010, doi: 10.1021/nn901585p.

[71] J. W. Kim *et al.*, “Clean and less defective transfer of monolayer graphene by floatation in hot water,” *Appl. Surf. Sci.*, vol. 508, no. 145057, Apr. 2020, doi: 10.1016/j.apsusc.2019.145057.

[72] W.-C. Lai, C.-N. Lin, Y.-C. Lai, P. Yu, G. C. Chi, and S.-J. Chang, “GaN-based light-emitting diodes with graphene/indium tin oxide transparent layer,” *Opt. Express*, vol. 22, no. 102, pp. A396–A401, Mar. 2014, doi: 10.1364/OE.22.00A396.

[73] S. Chandramohan *et al.*, “Performance evaluation of GaN light-emitting diodes using transferred graphene as current spreading layer,” *J. Appl. Phys.*, vol. 115, no. 5, p. 054503, Feb. 2014, doi: 10.1063/1.4863640.

[74] T. H. Seo *et al.*, “Enhanced Light Output Power of GaN Light-Emitting Diodes with Graphene Film as a Transparent Conducting Electrode,” *Jpn. J. Appl. Phys.*, vol. 50, no. 12R, p. 125103, Dec. 2011, doi: 10.1143/JJAP.50.125103.

[75] J.-H. Min *et al.*, “Effect of p-GaN hole concentration on the stabilization and performance of a graphene current spreading layer in near-ultraviolet light-emitting diodes,” *Curr. Appl. Phys.*, vol. 16, no. 10, pp. 1382–1387, Oct. 2016, doi: 10.1016/j.cap.2016.08.006.

[76] H. Zhong *et al.*, “Graphene in ohmic contact for both n-GaN and p-GaN,” *Appl. Phys. Lett.*, vol. 104, no. 21, p. 212101, May 2014, doi: 10.1063/1.4880732.

[77] D.-H. Youn, Y.-J. Yu, H. Choi, S.-H. Kim, S.-Y. Choi, and C.-G. Choi, "Graphene transparent electrode for enhanced optical power and thermal stability in GaN light-emitting diodes," *Nanotechnology*, vol. 24, no. 7, p. 075202, Jan. 2013, doi: 10.1088/0957-4484/24/7/075202.

[78] T. Tan Pham *et al.*, "How do the doping concentrations of N and B in graphene modify the water adsorption?," *RSC Adv.*, vol. 11, no. 32, pp. 19560–19568, 2021, doi: 10.1039/D1RA01506K.

[79] J. Kierdaszuk *et al.*, "Properties of graphene deposited on GaN nanowires: influence of nanowire roughness, self-induced nanogating and defects," *Beilstein J. Nanotechnol.*, vol. 12, no. 1, pp. 566–577, Jun. 2021, doi: 10.3762/bjnano.12.47.

[80] M. Tchernycheva *et al.*, "InGaN/GaN Core–Shell Single Nanowire Light Emitting Diodes with Graphene-Based P-Contact," *Nano Lett.*, vol. 14, no. 5, pp. 2456–2465, May 2014, doi: 10.1021/nl5001295.

[81] I. M. Høiaas *et al.*, "GaN/AlGaN Nanocolumn Ultraviolet LED using Double-Layer Graphene as Substrate and Transparent Electrode," *Nano Lett.*, vol. 19, Jan. 2019, doi: 10.1021/acs.nanolett.8b04607.

[82] H. Zhang, J. Mischke, W. Mertin, and G. Bacher, "Graphene as a Transparent Conductive Electrode in GaN-Based LEDs," *Materials*, vol. 15, p. 2203, Mar. 2022, doi: 10.3390/ma15062203.

[83] A. Liudi Mulyo *et al.*, "Vertical GaN nanocolumns grown on graphene intermediated with a thin AlN buffer layer," *Nanotechnology*, vol. 30, no. 1, p. 015604, Jan. 2019, doi: 10.1088/1361-6528/aae76b.

[84] A. Liudi Mulyo, M. K. Rajpalke, P. E. Vullum, H. Weman, K. Kishino, and B.-O. Fimland, "The influence of AlN buffer layer on the growth of self-assembled GaN nanocolumns on graphene," *Sci. Rep.*, vol. 10, no. 1, Art. no. 1, Jan. 2020, doi: 10.1038/s41598-019-55424-z.

[85] S. Fernández-Garrido *et al.*, "Molecular Beam Epitaxy of GaN Nanowires on Epitaxial Graphene," *Nano Lett.*, vol. 17, no. 9, pp. 5213–5221, Sep. 2017, doi: 10.1021/acs.nanolett.7b01196.

[86] E. F. Schubert, *Light-Emitting Diodes*, 2nd ed. Cambridge: Cambridge University Press, 2006. doi: 10.1017/CBO9780511790546.

[87] S. Nakamura, "Background story of the invention of efficient blue InGaN light emitting diodes (Nobel Lecture)," *Ann. Phys.*, vol. 527, no. 5–6, pp. 335–349, 2015, doi: 10.1002/andp.201500801.

[88] L. Rigutti and M. Tchernycheva, “Chapter 15 - Electrical and Electro-Optical Characterization of Semiconductor Nanowires,” in *Characterization of Semiconductor Heterostructures and Nanostructures (Second Edition)*, C. Lamberti and G. Agostini, Eds. Oxford: Elsevier, 2013, pp. 641–684. doi: 10.1016/B978-0-444-59551-5.00015-7.

[89] N. T. Kalyani, H. Swart, and S. J. Dhoble, “Chapter 9 - Organic Light-Emitting Diode Fabrication and Characterization Techniques,” in *Principles and Applications of Organic Light Emitting Diodes (OLEDs)*, N. T. Kalyani, H. Swart, and S. J. Dhoble, Eds. Woodhead Publishing, 2017, pp. 227–252. doi: 10.1016/B978-0-08-101213-0.00009-6.

[90] G. B. Nair and S. J. Dhoble, “2 - Fundamentals of LEDs,” in *The Fundamentals and Applications of Light-Emitting Diodes*, G. B. Nair and S. J. Dhoble, Eds. Woodhead Publishing, 2021, pp. 35–57. doi: 10.1016/B978-0-12-819605-2.00002-1.

[91] H. Parimoo, J. Lu, and S. Zhao, “Deep Ultraviolet Light Emission from AlGaN Nanowires with Graphene Electrode,” in *2021 Photonics North (PN)*, May 2021, pp. 1–1. doi: 10.1109/PN52152.2021.9597929.

[92] M. Biswas, V. Chavan, S. Zhao, Z. Mi, and S. Chakrabarti, “Passivation of Surface States of AlGaN Nanowires Using H3PO4 Treatment To Enhance the Performance of UV-LEDs and Photoanodes,” *ACS Appl. Nano Mater.*, vol. 1, no. 4, pp. 1968–1975, Apr. 2018, doi: 10.1021/acsanm.8b00447.

[93] F. Giubileo, A. D. Bartolomeo, Y. Zhong, S. Zhao, and M. Passacantando, “Field emission from AlGaN nanowires with low turn-on field,” *Nanotechnology*, vol. 31, no. 47, p. 475702, Nov. 2020, doi: 10.1088/1361-6528/abaf22.

[94] Y. Bleu, F. Bourquard, A.-S. Loir, V. Barnier, F. Garrelie, and C. Donnet, “Raman study of the substrate influence on graphene synthesis using a solid carbon source via rapid thermal annealing,” *J. Raman Spectrosc.*, vol. 50, pp. 1630–1641, 2019, doi: 10.1002/jrs.5683.

[95] K. H. Li, X. Liu, Q. Wang, S. Zhao, and Z. Mi, “Ultralow-threshold electrically injected AlGaN nanowire ultraviolet lasers on Si operating at low temperature,” *Nat. Nanotechnol.*, vol. 10, no. 2, Art. no. 2, Feb. 2015, doi: 10.1038/nnano.2014.308.

[96] S. Zhao *et al.*, “Three-Dimensional Quantum Confinement of Charge Carriers in Self-Organized AlGaN Nanowires: A Viable Route to Electrically Injected Deep Ultraviolet Lasers,” *Nano Lett.*, vol. 15, no. 12, pp. 7801–7807, Dec. 2015, doi: 10.1021/acs.nanolett.5b02133.

[97] H. Parimoo, Q. Zhang, M. Vafadar, J. Sivasundarampillai, and S. Zhao, “AlGaN nanowire deep ultraviolet light emitting diodes with graphene electrode,” *Appl. Phys. Lett.*, vol. 120, no. 17, p. 171108, Apr. 2022, doi: 10.1063/5.0092599.

[98] H. Cao *et al.*, “Electronic transport in chemical vapor deposited graphene synthesized on Cu: Quantum Hall effect and weak localization,” *Appl. Phys. Lett.*, vol. 96, no. 12, p. 122106, Mar. 2010, doi: 10.1063/1.3371684.

[99] S. Kim, I. S. Park, H.-J. Kwon, W.-J. Chang, and S. W. Lee, “Current on/off ratio enhancement through the electrical burning process in ambient with/without oxygen for the generation of high-performance aligned single-walled carbon nanotube field effect transistors,” *Appl. Phys. Lett.*, vol. 97, no. 17, p. 173102, Oct. 2010, doi: 10.1063/1.3504689.

[100] X. Langston and K. E. Whitener, “Graphene Transfer: A Physical Perspective,” *Nanomaterials*, vol. 11, no. 11, Art. no. 11, Nov. 2021, doi: 10.3390/nano11112837.

[101] S. Ullah *et al.*, “Graphene transfer methods: A review,” *Nano Res.*, vol. 14, no. 11, pp. 3756–3772, Nov. 2021, doi: 10.1007/s12274-021-3345-8.

[102] Y. Song, W. Zou, Q. Lu, L. Lin, and Z. Liu, “Graphene Transfer: Paving the Road for Applications of Chemical Vapor Deposition Graphene.,” *Small*, 2021, doi: 10.1002/smll.202007600.

[103] X. Liang *et al.*, “Toward Clean and Crackless Transfer of Graphene,” *ACS Nano*, vol. 5, no. 11, pp. 9144–9153, Nov. 2011, doi: 10.1021/nn203377t.

[104] Y. Chen, X.-L. Gong, and J.-G. Gai, “Progress and Challenges in Transfer of Large-Area Graphene Films,” *Adv. Sci.*, vol. 3, no. 8, p. 1500343, 2016, doi: 10.1002/advs.201500343.

[105] W. S. Leong *et al.*, “Paraffin-enabled graphene transfer,” *Nat. Commun.*, vol. 10, no. 1, Art. no. 1, Feb. 2019, doi: 10.1038/s41467-019-08813-x.

[106] N. Villa, J. D. Zapata, and D. Ramirez, “Paraffin wax assisted chemical vapor deposited graphene transfer method,” *Thin Solid Films*, vol. 721, p. 138556, Mar. 2021, doi: 10.1016/j.tsf.2021.138556.

[107] J. Lu, M. F. Vafadar, and S. Zhao, “Light extraction efficiency of AlGaN nanowire deep ultraviolet light-emitting diodes on Si with different photonic structures,” *J. Nanophotonics*, vol. 15, no. 3, p. 036002, Jul. 2021, doi: 10.1117/1.JNP.15.036002.